

1 **Supplemental Information for:**

2

3 **Transport-driven aerosol differences above and below the canopy of**
4 **a mixed deciduous forest**

5

6 Alexander A.T. Bui¹, Henry W. Wallace^{1, a}, Sarah Kavassalis², Hariprasad D. Alwe³, James H. Flynn⁴,
7 Matt H. Erickson^{4, b}, Sergio Alvarez⁴, Dylan B. Millet³, Allison L. Steiner⁵, Robert J. Griffin^{1, 6}

8 ¹ Department of Civil and Environmental Engineering, Rice University, Houston, TX, 77005, USA

9 ² Department of Chemistry, University of Toronto, Toronto, ON, M5S 3H6, Canada

10 ³ Department of Soil, Water, and Climate, University of Minnesota, St. Paul, MN 55108, USA

11 ⁴ Department of Earth and Atmospheric Sciences, University of Houston, Houston, TX, 77204, USA

12 ⁵ Department of Climate and Space Sciences and Engineering, University of Michigan, Ann Arbor, MI, 48109, USA

13 ⁶ Department of Chemical and Biomolecular Engineering, Rice University, Houston, TX, 77005, USA

14 ^a now at: Washington State Department of Ecology, Lacey, WA, 98503, USA

15 ^b now at: TerraGraphics Environmental Engineering, Pasco, WA, 99301, USA

16 *Correspondence to:* Robert J. Griffin (rob.griffin@rice.edu)

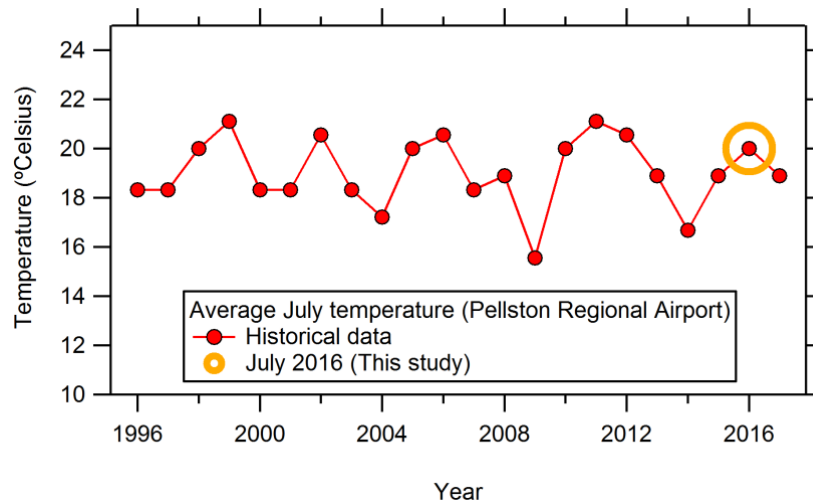


Figure S 1: Historical average July temperature data from the Pellston Regional Airport, where the yellow circle represents the July 2016 PROPHET-AMOS study period.

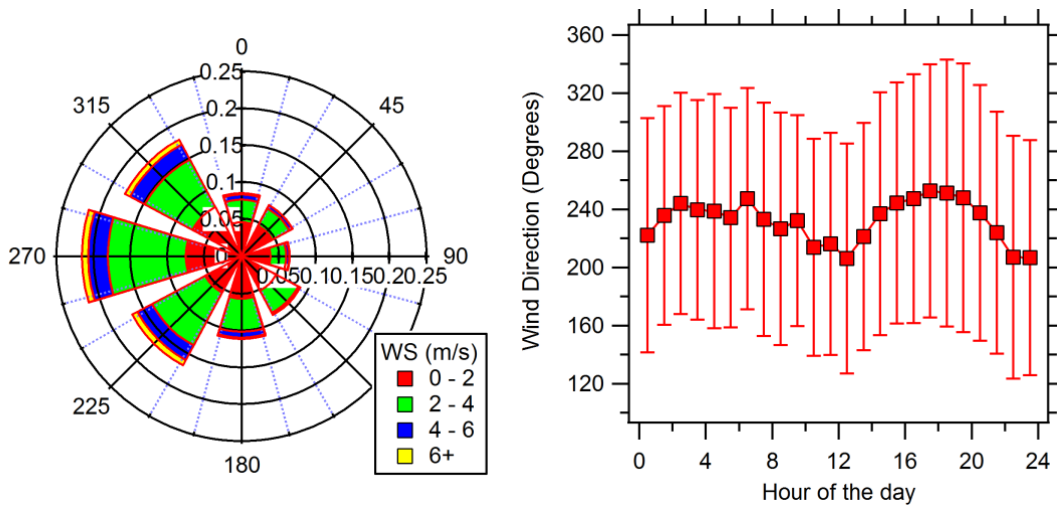


Figure S 2: (left) Wind rose (direction and speed) plot for July 2016 from the top of the PROPHET tower using weather station measurements from the University of Houston, (right) diurnal variation of wind direction from the top of the PROPHET tower, where squares represent medians and whiskers represent one standard deviation from the mean value.

1 **Table S 1: Table of measurements on board the University of Houston/Rice University Mobile Air Quality Laboratory (MAQL).**
2 **The MAQL was situated approximately 10 m to the east of the PROPHET tower.**

Species	Instrumentation	Institution	Sampling height (m)	Time resolution / Limit of detection
Non-refractory PM₁ size resolved composition	Aerodyne HR-ToF-AMS	Rice University	6, 30 ^a	30-40 sec (see main text) / Varies (see Table S3)
Ozone (O₃)	Thermo Electron Corp. 49C O ₃ Analyzer (ultraviolet photometry)	University of Houston	6	5 min. / 1.2 ppbv
Carbon monoxide (CO)	Los Gatos Research (high-resolution cavity enhanced direct-absorption spectroscopy)	University of Houston	6	5 min. / 4 ppbv
Sulfur dioxide (SO₂)	Thermo Fisher Scientific (pulsed fluorescence analyzer)	University of Houston	6	5 min. / 0.033 ppbv
Nitric oxides (NO, NO₂, NO_x), NO_y	Air Quality Design NO-NO ₂ -NO _x analyzers (high sensitivity chemiluminescence)	University of Houston	6	NO: 5 min. / 0.007 ppbv NO ₂ : 5 min. / 0.029 ppbv NO _y : 5 min. / 0.053 ppbv
Temp, RH, pressure, wind speed/direction	RM Young meteorological station	University of Houston	6	5 min. / N/A

3 ^a Sampling inlet height on the PROPHET tower.



2
3 **Figure S 3: Images taken during the PROPHET-AMOS 2016 campaign of the following: (left) PROPHET tower above the canopy**
4 **from atop the AmeriFlux tower facing south-southwest and (right) University of Houston/Rice University MAQL situated below**
5 **the canopy.**

1 **Table S 2: Table of measurements, institutions, and locations during the PROPHET-AMOS 2016 campaign. Sampling heights are based on height**
2 **above ground level on the PROPHET tower, unless otherwise noted.**

Species	Instrumentation/Method	Institution	Sampling height (m)	Time resolution / Limit of detection ^a
Nitric oxides (NO, NO₂)	Air Quality Design Dual-Channel Chemiluminescence detector (AQD NO _{xy}) ^b	University of Toronto	29	NO: 5 min. / 6 pptv NO ₂ : 5 min. / 12 pptv
Ozone (O₃)	Thermo Scientific 49C O ₃ analyzer	University of Colorado Boulder	27 ^c	1 min. / 1 ppbv ^c
Volatile organic compounds (VOCs)	High-resolution Proton Transfer Reaction-Quadrupole interface Time-Of-Flight mass spectrometer (PTR-QiTOF)	University of Minnesota	5, 9, 13, 17, 21, and 34 ^d	Benzene: 1 min. / 20 pptv Monoterpene: 1 min. / 23 pptv Isoprene: 1 min. / 41 pptv
Temperature, RH, pressure, wind speed/wind direction	Vaisala Humidity and temperature probe (HMP-60) and weather station	University of Houston	34	5 min. / N/A

3 ^a Detection limit calculated as 3 σ of the reported time-resolution averages of the zero/blank measurement periods, unless otherwise noted

4 ^b Identical instrumentation to that used at PROPHET tower in 2011, as described in Geddes and Murphy (2014)

5 ^c O₃ measurement was located at Department of Energy (DOE) AmeriFlux tower, located 132 m north-northeast of PROPHET tower (Carroll et al., 2001). Reported detection limit of the O₃ analyzer.

7 ^d Operation of the PTR-QiTOF during the PROPHET-AMOS 2016 campaign is described in Millet et al. (2018)

1 **Table S 3: Table of detection limits for NR-PM₁ species during the PROPHET-AMOS 2016 campaign.**

Species	Detection limit ^a (µg m⁻³)
SO ₄	0.0106
OA	0.1573
NO ₃	0.0073
NH ₄	0.0068
Chl	0.0064

2 ^a Detection limits of different NR-PM₁ species are calculated based on 3 times the standard deviation of mass concentrations of
3 5-minute averaged data during periods of HEPA-filtered air.

Positive matrix factorization analysis for above- and below-canopy OA

In the following sections, selection of the optimal number of PMF factors, SEED values, and FPEAK values will be discussed. This will be done first for the above-canopy OA data and second for the below-canopy OA data. Next, the factors for above-canopy and below-canopy OA data will be briefly described and interpreted.

Above-canopy PMF solution

Table S 4 summarizes the PMF factor selection for the above-canopy OA data. Table S 5 and Table S 6 present correlation coefficients between different PMF factor solutions and time series of external data and reference mass spectra, respectively. Correlation coefficients presented here represent Pearson correlation coefficients and will be hereafter referred to as correlation coefficients or R.

A one-factor PMF solution results in an oxygenated OA (OOA). However, time series of model residuals indicate large residuals not fit by the model (as shown in the top-left panel of Figure S 4). Factor time series and mass spectra are shown for the two-factor, three-factor, four-factor, and five-factor solution in Figure S 5, Figure S 6, Figure S 7, and Figure S 8, respectively.

A two-factor PMF solution (Figure S 5) results in a more-oxidized oxygenated organic aerosol (MO-OOA) and a less oxidized oxygenated organic aerosol (LO-OOA), each of which has a distinct time series. The two-factor solution introduces a decrease in Q/Q_{exp} (Table S 4) and a reduction in the structure of the time series of model residuals compared to the one-factor solution (Figure S 4). As shown in Table S 5, the MO-OOA-related factor correlates with time series of AVOCs (i.e., toluene, benzenes, and C₂-benzenes) ($R > 0.40$), SO₄ ($R = 0.72$), NH₄ ($R = 0.77$), and NO₃ ($R = 0.73$) while the LO-OOA correlates most strongly with the f_{C₅H₆O} AMS tracer ($R = 0.63$) for isoprene-epoxydiol derived SOA (IEPOX-OA).

Increasing the number of the factors to three (Figure S 6) yields one MO-OOA and two LO-OOA factors with distinct factor time series. The addition of a third factor increases correlations between factors and time series of external data compared to the previous solution (trace gases and NR-PM₁ (Table S 5) and reference mass spectra (Table S 6). Specifically, this solution yields an LO-OOA (Factor 2) with moderate correlations with unidentified terpene oxidation products listed in Table S 7 ($R > 0.4$, as shown in Table S 8). The three-factor solution introduces a decrease in Q/Q_{exp} and a further reduction in the structure of the time series of model residuals (Figure S 4).

A four-factor solution (Figure S 7) yields an additional factor that is less interpretable and less physically meaningful due to the noise of the time series of the additional factor (i.e., Factor 4 in the four-factor solution). No increases in correlation coefficients with external data are observed with the addition of this factor. The reduction in Q/Q_{exp} with the addition of this factor is not as large as the previous solution (-0.09 for previous solution versus -0.05 for this solution). Inspection of the model residuals of the four-factor solution indicates that the additional factor does not substantially decrease the structure of the residuals (Figure S 4).

A five-factor solution (Figure S 8) yields two MO-OOA factors and three LO-OOA factors (Factor 2/LO-OOA has a distinct peak at m/z 82). However, the time series of the additional factor (Factor 5) is not physically meaningful and/or interpretable due to noise. Insufficient supporting evidence from correlations with external data and reference mass spectra precludes the addition of Factor 5 and Factor 2 (LO-OOA factor with a distinct peak at m/z 82).

For the four-factor solution, the similarity of the mass spectra of Factor 3 and Factor 4 ($R = 0.99$), the similarity of the mass spectra of Factor 1 and Factor 3 ($R = 0.96$) (as shown in Figure S 9), and the lack of physical meaning regarding the time series of Factor 4 indicate that the addition of a new factor exhibits factor splitting. Factor splitting behavior occurs when mass spectra or time series from a real factor are split into two new factors; this has been observed in previous PMF studies when additional factors are added (Ulbrich et al., 2009). Correlation of mass spectra within the five-factor solution also indicates similarity between Factor 1, 3, 4, and 5 (clustering of points at the bottom right-hand side of Figure S 9, which is indicative of factor splitting. No strong change in the slope of Q/Q_{exp} is observed between the four- and five-factor solutions. Further increasing the number of factors between 6 and 8 does not result in significant reductions in Q/Q_{exp} and produces additional meaningless factors. Taken together, this information indicates that the three-factor solution is the optimal solution for this dataset.

The effects of the pseudorandom starting values for the PMF2 algorithm is analyzed by initializing the PMF model at 50 different starting points (SEEDS) in increments of 1 for the three-factor solution. As shown in Figure S 10, this analysis indicates that values of Q/Q_{exp} and the mass fraction of the factors do not change across SEEDS, which is indicative of a stable

1 solution (top right and middle panels of Figure S 10 respectively). The rotational ambiguity of the mass spectra is analyzed by
2 changing the FPEAK parameter between -1.0 and 1.0 in increments of 0.2 for the three-factor solution (Figure S 10). Table S 9
3 displays the FPEAK analysis results where correlations to reference mass spectra are shown at different FPEAK values. No
4 significant or consistent increase in correlation is observed when compared to the solution at $FPEAK = 0$ (Table S 6).
5 Furthermore, an inspection of the model residuals at each time step and m/z indicates that no improvements in model residuals
6 are observed across different FPEAK values. Therefore, the FPEAK analysis indicates that $FPEAK = 0$ is the most appropriate
7 solution. Based on this information, the three-factor solution ($FPEAK = 0$ and $SEED = 0$) is the optimal solution for the above-
8 canopy OA dataset. Model residual diagnostic plots for each m/z and time step for the optimal three-factor solution ($FPEAK =$
9 0 , $SEED = 0$) along with a comparison of the measured and reconstructed OA mass are shown in Figure S 11.

10 Results from 100 bootstrapping runs of the three-factor solution at $SEED = 0$ and $FPEAK = 0$ are shown in Figure S 12.
11 Bootstrapping analysis indicates that the statistical uncertainties of the time series and mass spectra of all factors are small in
12 comparison to the time series and mass spectra signals. This type of bootstrapping analysis allows us to conclude that the three-
13 factor solution results are robust over 100 bootstrapping runs. The high-resolution mass spectra, time series of factor mass
14 concentrations, and time series of fractional contributions of OA factors to total OA for the optimal above-canopy OA solution is
15 shown in Figure S 13.

16

1 Table S 4: Summary of PMF factor selection for above-canopy OA.

# Factors	FPEAK	SEED	$Q/Q_{expected}$	$\Delta Q/Q_{expected}^1$	Solution Description
1	0	0	4.41966	N/A	One-factor solution.
2	0	0	4.25992	-0.15974	Two-factor solution.
3	0	0 to 50 in steps of 1	4.16830-4.16831	---	Varying the three-factor solution at different starting points (seeds) indicates that the solution is stable, with similar factor mass spectra and time series.
3	-1.0 to 1.0 in increments of 0.2	0	4.16831-4.17102	---	Each factor of the three-factor solution display distinct time series and mass spectra.
3	0	0	4.16831	-0.09161	Optimal three-factor solution yields factors with distinct time series, and correlations with external time series and mass spectra data.
4	0	0	4.11803	-0.05028	Four-factor solution.
5	0	0	4.07985	-0.03818	Five-factor solution.
6 to 8	0	0	4.05134 to 4.00136	-0.02851 to -0.02389	For solutions greater than five-factor solutions, additional physically meaningless factors are extracted.

2

3

1 S 5: Summary of different PMF factor solutions for above-canopy OA data and time series correlations with external data. Table
 2 entries shaded in gray represent correlation coefficients that are greater than or equal to 0.40.

Two-factor		Three-factor			Four-factor				Five-factor					
VOCs ^a , R Time Series														
Factor #	1	2	1	2	3	1	2	3	4	1	2	3	4	5
Acetaldehyde	0.40	0.35	0.45	0.02	0.44	0.44	0.43	0.17	0.27	0.19	0.39	0.55	0.23	0.24
Acetonitrile	0.46	0.04	0.54	-0.20	0.24	0.53	0.23	-0.07	0.15	0.25	0.18	0.57	-0.04	0.13
Acetone	0.57	0.11	0.60	0.01	0.22	0.59	0.20	0.08	0.22	0.25	0.15	0.68	0.12	0.18
Benzene	0.67	0.01	0.67	0.07	0.11	0.67	0.11	0.11	0.13	0.47	0.06	0.65	0.05	0.11
C ₂ .benzenes	0.42	0.09	0.34	0.37	-0.00	0.34	0.00	0.30	0.1	0.32	-0.02	0.30	0.21	0.11
C ₃ .benzenes	0.37	0.16	0.30	0.38	0.05	0.30	0.06	0.33	0.12	0.27	0.04	0.28	0.26	0.13
C ₄ .benzenes	0.32	0.00	0.22	0.38	-0.13	0.22	-0.12	0.26	0.05	0.25	-0.14	0.18	0.16	0.05
C ₅ .carbonyls	0.70	0.00	0.74	-0.03	0.16	0.73	0.14	0.04	0.15	0.44	0.09	0.75	0.02	0.13
C ₄ .carbonyls	0.71	-0.07	0.73	-0.05	0.09	0.73	0.08	0.01	0.10	0.48	0.03	0.72	-0.04	0.09
C ₆ .carbonyls	0.48	0.26	0.52	0.05	0.35	0.51	0.34	0.16	0.24	0.27	0.3	0.58	0.19	0.21
Isoprene	0.03	0.26	0.06	0.00	0.28	0.06	0.27	0.09	0.16	-0.07	0.25	0.15	0.17	0.14
Methanol	0.47	0.15	0.51	-0.03	0.27	0.50	0.25	0.06	0.21	0.21	0.21	0.58	0.11	0.18
Methylfuran	0.22	0.37	0.22	0.19	0.35	0.22	0.35	0.25	0.25	0.10	0.32	0.30	0.29	0.24
Monoterpenes	0.11	0.18	0.05	0.35	0.04	0.04	0.04	0.28	0.11	0.03	0.03	0.08	0.27	0.10
MVK+MACR	0.20	0.32	0.20	0.17	0.30	0.20	0.30	0.23	0.20	0.11	0.28	0.25	0.26	0.19
Toluene	0.43	0.11	0.37	0.31	0.05	0.37	0.04	0.26	0.13	0.3	0.02	0.36	0.2	0.12
Aromatics	0.46	0.07	0.38	0.34	-0.00	0.38	0.00	0.28	0.11	0.34	-0.03	0.35	0.19	0.11
Trace Gases, R Time Series														
Factor #	1	2	1	2	3	1	2	3	4	1	2	3	4	5
NO ₂ ^b	0.33	-0.08	0.27	0.2	-0.12	0.28	-0.1	0.16	-0.04	0.32	-0.11	0.19	0.04	-0.03
NO ^b	0.06	0.02	0.01	0.19	-0.07	0.01	-0.06	0.14	-0.01	0.11	-0.04	-0.04	0.07	0.00
O ₃ ^c	0.60	-0.43	0.64	-0.22	-0.20	0.63	-0.22	-0.25	-0.04	0.38	-0.27	0.59	-0.31	-0.06
NR-PM ₁ , R Time Series														
Factor #	1	2	1	2	3	1	2	3	4	1	2	3	4	5
fC ₅ H ₆ O	-	0.63	-0.48	0.02	0.58	-0.47	0.60	0.22	0.14	-0.35	0.64	-0.39	0.34	0.15
SO ₄	0.72	-0.13	0.79	-0.25	0.15	0.79	0.16	-0.08	0.014	0.62	0.12	0.72	-0.16	0.01
NH ₄	0.77	-0.18	0.84	-0.22	0.09	0.84	0.10	-0.08	0.01	0.63	0.05	0.77	-0.17	0.00
NO ₃	0.73	-0.08	0.72	0.11	0.02	0.72	0.02	0.14	0.07	0.55	-0.04	0.68	0.05	0.06
Chl	0.28	-0.05	0.29	0.00	0.00	0.28	0.00	0.01	0.04	0.18	-0.02	0.28	-0.00	0.03

3 ^a VOCs measured using University of Minnesota's PTR- QITOF from the 34-m inlet at the top of the PROPHET tower.

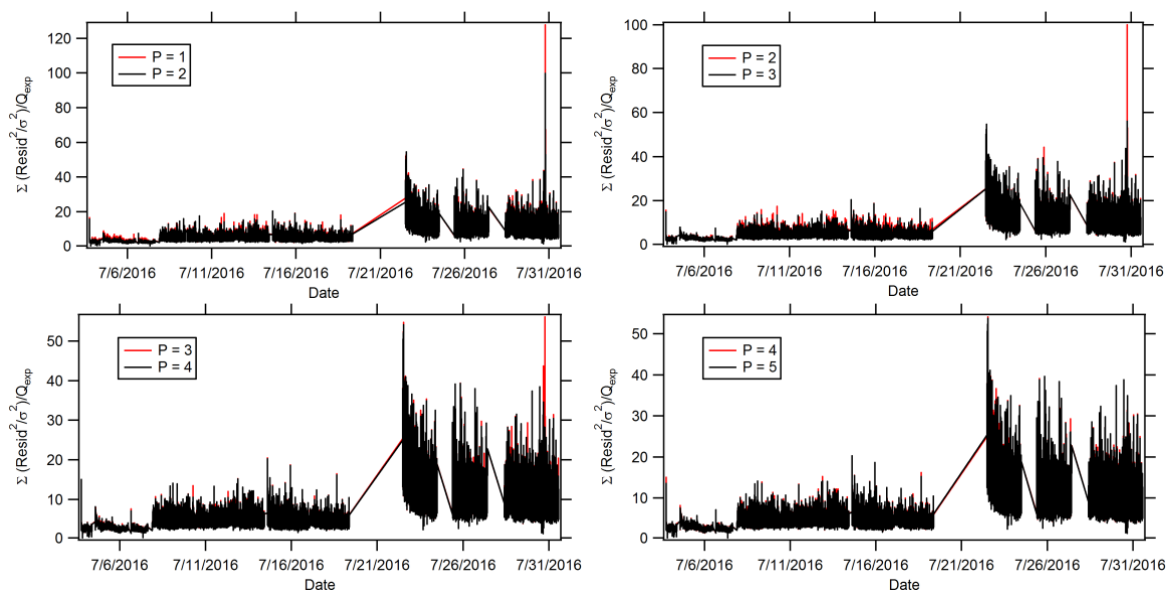
4 ^b NO_x measured from NCAR instruments from the 34-m inlet at the top of the PROPHET tower.

5 ^c O₃ measured from the University of Colorado Boulder instruments from the 27-m inlet at the AmeriFlux tower.

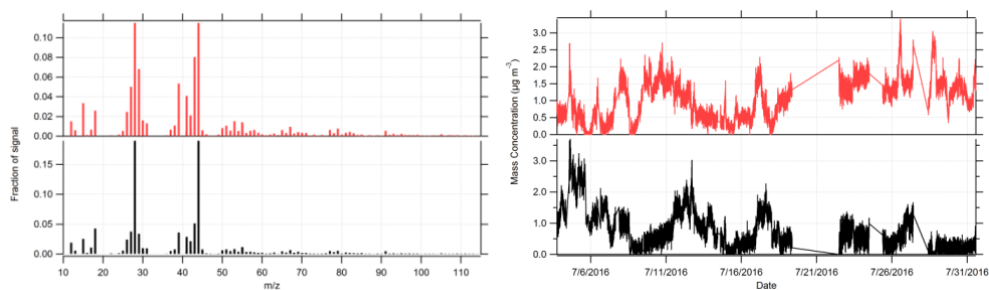
1 Table S 6: Summary of PMF factor solutions for above-canopy OA data and correlation coefficients with reference mass spectra
2 from the unit-mass resolution and high-resolution AMS spectral database from the Jimenez Group at University of Colorado
3 Boulder, where table entries shaded in gray correlation coefficients that are greater than or equal to 0.80. PMF solutions with
4 SEED = 0 and FPEAK = 0 are shown. Further details on the mass spectral database can be found in the literature (Ulbrich et al.,
5 2009), and at the following URL: <http://cires.colorado.edu/jimenez-group/HRAMSSd/>.

	2-factor		3-factor			4-factor				5-factor				
	<i>Reference Mass Spectra, $R_{\text{Mass Spectra}}$</i>													
	1	2	1	2	3	1	2	3	4	1	2	3	4	5
MO-OOA ^a	0.86	0.81	0.85	0.84	0.79	0.84	0.65	0.84	0.84	0.85	0.51	0.83	0.83	0.84
LO-OOA ^a	0.68	0.86	0.62	0.82	0.86	0.61	0.82	0.82	0.80	0.72	0.73	0.58	0.84	0.82
BBOA ^a	0.59	0.82	0.53	0.75	0.84	0.51	0.88	0.75	0.70	0.69	0.84	0.46	0.75	0.72
HOA ^a	0.34	0.52	0.29	0.48	0.53	0.27	0.53	0.48	0.47	0.38	0.49	0.25	0.50	0.49
IEPOX-OA ^b	0.74	0.88	0.70	0.84	0.88	0.68	0.85	0.84	0.81	0.80	0.77	0.64	0.84	0.82
IEPOX-OA ^c	0.73	0.92	0.69	0.85	0.95	0.68	0.98	0.85	0.81	0.80	0.90	0.64	0.85	0.82
82Fac ^d	0.67	0.55	0.53	0.63	0.68	0.52	0.72	0.63	0.62	0.55	0.68	0.52	0.65	0.63
91Fac ^d	0.84	0.70	0.65	0.81	0.84	0.64	0.80	0.81	0.80	0.74	0.72	0.61	0.82	0.81

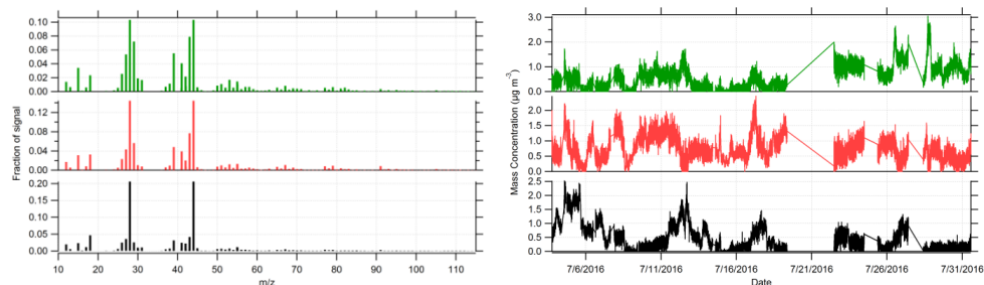
- 6 ^a Average MS from multiple ambient data sets (Ng et al., 2011).
7 ^b Atlanta, GA in Summer 2011, Source: (Budisulistiorini et al., 2013).
8 ^c Southern Oxidant and Aerosol Study (SOAS) in Centreville, AL in Summer 2013 (Hu et al., 2015).
9 ^d Malaysian Borneo rainforest in 2008 (Robinson et al., 2011a).



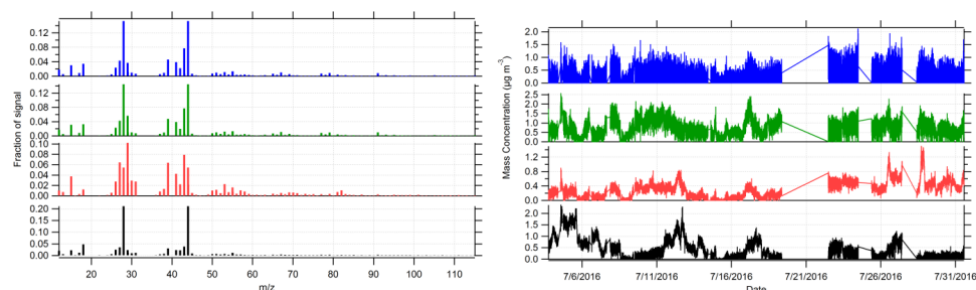
13 Figure S 4: Q/Q_{exp} (i.e., $\Sigma(\text{Resid}^2/\sigma^2)/Q_{\text{exp}}$) contribution for each time step for different number of factors (where $P = \#$ of factors)
14 for above-canopy OA data. Each plot compares Q/Q_{exp} at each time step between the following factors for: (top left) one- and two-
15 factor solutions, (top right) two- and three-factor solutions, (bottom left) three- and four-factor solutions, and (bottom right) four-
16 and five-factor solutions. It should be noted that the range of the y-axis changes between each set of plots.



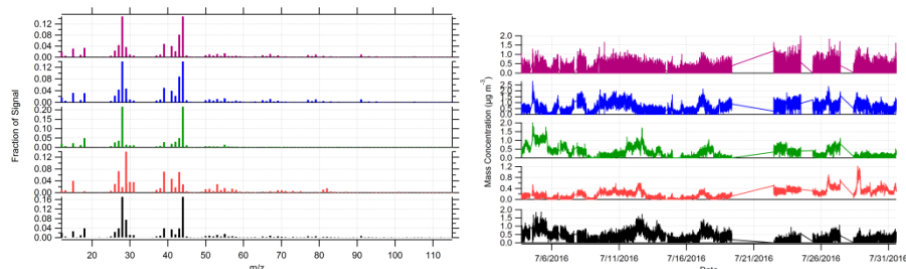
1
2 **Figure S 5: (left) Mass spectra and (right) time series for the two-factor solution for above-canopy OA data, where Factor 2 and**
3 **Factor 1 are shown from top to bottom, respectively.**



4
5 **Figure S 6: (left) Mass spectra and (right) time series for the three-factor solution for above-canopy OA data, where Factor 3,**
6 **Factor 2, and Factor 1 are shown from top to bottom, respectively.**



7
8 **Figure S 7: (left) Mass spectra and (right) time series for the four-factor solution for above-canopy OA data, where Factors 4**
9 **through 1 are shown from top to bottom, respectively.**



10
11 **Figure S 8: (left) Mass spectra and (right) time series for the five-factor solution for above-canopy OA data, where Factors 5**
12 **through 1 are shown from top to bottom, respectively.**

1 Table S 7: Summary of the VOCs measured by University of Minnesota's PTR-QiTOF from the 34-m inlet at the top of the
2 PROPHET tower. The relative variability of these measured species is used for PMF analysis.

Mass	Ion Formula	Exact Mass	Additional Notes
47.011	CH_3O_2^+	47.01276	Formic acid
47.0478	$\text{C}_2\text{H}_7\text{O}^+$	47.04914	Ethanol
57.034	$\text{C}_3\text{H}_5\text{O}^+$	57.03349	Acrolein
61.029	$\text{C}_2\text{H}_5\text{O}_2^+$	61.02841	Acetic acid/glycoaldehyde
73.02691	$\text{C}_3\text{H}_5\text{O}_2^+$	73.02841	Methylglyoxal/acrylic acid
75.0446	$\text{C}_3\text{H}_7\text{O}_2^+$	75.04406	Hydroxyacetone/propanoic acid
113.05511	$\text{C}_6\text{H}_9\text{O}_2^+$	113.0594	Likely terpene oxidation product
115.07355	$\text{C}_6\text{H}_{11}\text{O}_2^+$	115.0754	Likely terpene oxidation product
127.07339	$\text{C}_7\text{H}_{11}\text{O}_2^+$	127.0754	Likely terpene oxidation product
127.10961	$\text{C}_8\text{H}_{15}\text{O}^+$	127.1117	Likely terpene oxidation product
129.08796	$\text{C}_7\text{H}_{13}\text{O}_2^+$	129.091	Likely terpene oxidation product
139.11197	$\text{C}_9\text{H}_{15}\text{O}^+$	139.1117	Likely terpene oxidation product
151.11044	$\text{C}_{10}\text{H}_{15}\text{O}^+$	151.1117	Likely terpene oxidation product
169.12196	$\text{C}_{10}\text{H}_{17}\text{O}_2^+$	169.223	Likely terpene oxidation product
205.1956	$\text{C}_{15}\text{H}_{25}^+$	205.1951	Sesquiterpenes
237.18584	$\text{C}_{15}\text{H}_{25}\text{O}_2^+$	237.1849	Likely sesquiterpene oxidation product
253.1774	$\text{C}_{15}\text{H}_{25}\text{O}_3^+$	253.1798	Likely sesquiterpene oxidation product

3

1 Table S 8: Summary of correlation coefficients between different PMF factor solutions for above-canopy OA data and VOC
 2 masses measured by University of Minnesota’s PTR-QiTOF. Table entries shaded in gray represent correlation coefficients that
 3 are greater than or equal to 0.40. PMF solutions with SEED = 0 and FPEAK = 0 are shown.

	Two-factor		Three-factor			Four-factor				Five-factor				
VOCs Masses from PTR-QiTOF, R Time Series														
Factor #	1	2	1	2	3	1	2	3	4	1	2	3	4	5
47.011	0.32	0.30	0.38	-0.03	0.40	0.37	0.39	0.12	0.22	0.14	0.35	0.47	0.19	0.19
47.0478	0.32	0.05	0.33	0.02	0.11	0.32	0.10	0.07	0.08	0.19	0.08	0.34	0.06	0.08
57.034	0.45	0.17	0.48	0.00	0.27	0.48	0.27	0.11	0.16	0.26	0.23	0.53	0.13	0.14
61.029	0.41	0.27	0.48	-0.08	0.41	0.47	0.40	0.08	0.24	0.21	0.36	0.56	0.14	0.21
73.02691	0.44	0.27	0.48	0.01	0.37	0.47	0.36	0.14	0.24	0.25	0.32	0.55	0.17	0.21
75.0446	0.64	-0.00	0.66	0.03	0.11	0.66	0.11	0.09	0.09	0.47	0.07	0.63	0.03	0.07
113.05511	0.28	0.41	0.34	0.01	0.50	0.33	0.49	0.18	0.28	0.09	0.45	0.46	0.26	0.25
115.07355	0.60	0.10	0.63	0.01	0.22	0.62	0.22	0.10	0.17	0.38	0.17	0.65	0.09	0.15
127.07339	0.37	0.30	0.37	0.20	0.29	0.36	0.29	0.27	0.21	0.21	0.26	0.43	0.28	0.19
127.10961	0.31	0.15	0.31	0.13	0.16	0.30	0.16	0.16	0.13	0.18	0.13	0.34	0.16	0.11
129.08796	0.55	0.16	0.54	0.19	0.19	0.53	0.19	0.23	0.18	0.34	0.14	0.57	0.20	0.16
139.11197	0.14	0.42	0.07	0.46	0.25	0.07	0.25	0.44	0.21	0.06	0.24	0.13	0.44	0.21
151.11044	0.33	0.13	0.24	0.42	0.00	0.24	0.00	0.32	0.12	0.24	-0.02	0.23	0.26	0.12
169.12196	0.28	0.25	0.20	0.45	0.10	0.20	0.10	0.38	0.16	0.19	0.09	0.22	0.34	0.15
205.1956	0.15	0.12	0.10	0.28	0.01	0.10	0.01	0.22	0.08	0.09	0.00	0.11	0.19	0.08
237.18584	0.27	0.04	0.23	0.18	0.00	0.23	0.00	0.14	0.07	0.18	-0.01	0.23	0.10	0.06
253.1774	0.11	0.05	0.10	0.06	0.04	0.10	0.05	0.07	0.04	0.07	0.04	0.11	0.06	0.03

4

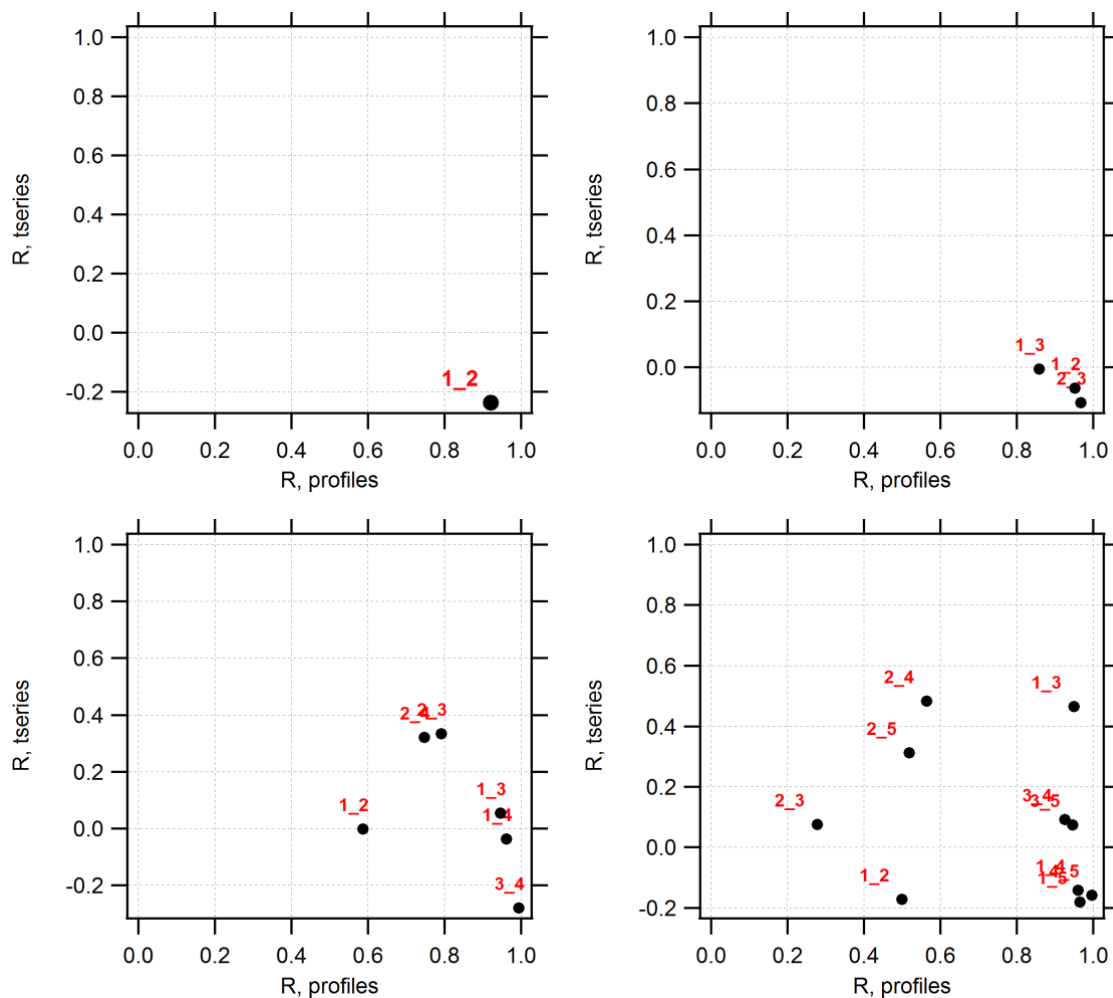
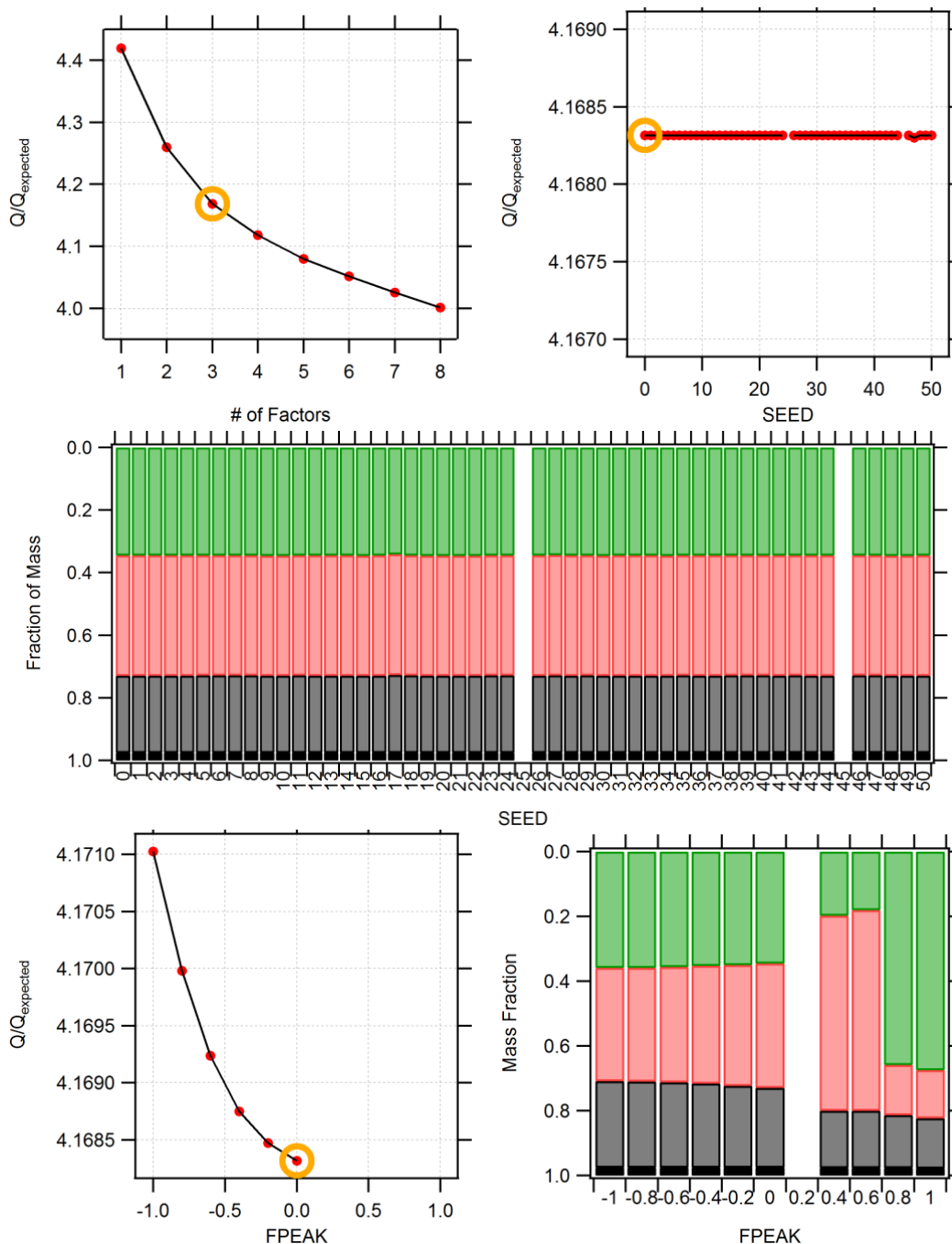


Figure S 9: Factor correlation plots based on factor time series ($R, \text{tseries}$) and factor mass spectra (“ $R, \text{profiles}$ ”) of above-canopy OA data for the following: (top left) two-factor solution, (top right) three-factor solution, (bottom left) four-factor solution, (bottom right) five-factor solution. Correlation coefficients are shown with black circles, and are labeled in red as $R_{i,j}$, where i and j represent the factor numbers i and j within a given PMF solution.



1 **Table S 9: Summary of correlation coefficients of the three-factor PMF solution for above-canopy OA data with reference mass**
2 **spectra using FPEAK analysis, where FPEAK ranges from -1.0 to -0.2 in increments of 0.2. PMF solutions with FPEAK values >**
3 **0.0 did not achieve convergence and are not shown. Reference mass spectra from the unit-mass resolution and high-resolution**
4 **AMS spectral database are used for comparison to the above-canopy PMF factor solutions at different FPEAK values (Ulbrich et**
5 **al., 2009).**

FPEAK	-1.0			-0.8			-0.6		
	1	2	3	1	2	3	1	2	3
MO-OOA^a	0.85	0.84	0.80	0.85	0.84	0.80	0.85	0.84	0.79
LO-OOA^a	0.66	0.82	0.86	0.65	0.82	0.86	0.65	0.82	0.86
BBOA^a	0.57	0.75	0.82	0.56	0.75	0.83	0.56	0.75	0.83
HOA^a	0.32	0.48	0.52	0.31	0.48	0.52	0.31	0.48	0.52
IEPOX-OA^b	0.73	0.84	0.88	0.72	0.84	0.88	0.72	0.84	0.88
IEPOX-OA^c	0.72	0.85	0.94	0.71	0.85	0.94	0.71	0.85	0.94
82Fac^d	0.54	0.63	0.67	0.54	0.63	0.67	0.54	0.63	0.67
91Fac^d	0.68	0.81	0.84	0.68	0.81	0.84	0.67	0.81	0.84

6

FPEAK	-0.4			-0.2		
	1	2	3	1	2	3
MO-OOA^a	0.85	0.84	0.79	0.85	0.84	0.79
LO-OOA^a	0.64	0.82	0.86	0.63	0.82	0.86
BBOA^a	0.55	0.75	0.83	0.54	0.75	0.83
HOA^a	0.30	0.48	0.53	0.29	0.48	0.53
IEPOX-OA^b	0.71	0.84	0.88	0.70	0.84	0.88
IEPOX-OA^c	0.70	0.85	0.94	0.70	0.85	0.95
82Fac^d	0.53	0.63	0.68	0.53	0.63	0.68
91Fac^d	0.67	0.81	0.84	0.66	0.81	0.84

7 ^a Average MS from multiple ambient data sets (Ng et al., 2011).

8 ^b Atlanta, GA in Summer 2011, Source: (Budisulistiorini et al., 2013).

9 ^c Southern Oxidant and Aerosol Study (SOAS) in Centreville, AL in Summer 2013 (Hu et al., 2015).

10 ^d Malaysian Borneo rainforest in 2008 (Robinson et al., 2011a).

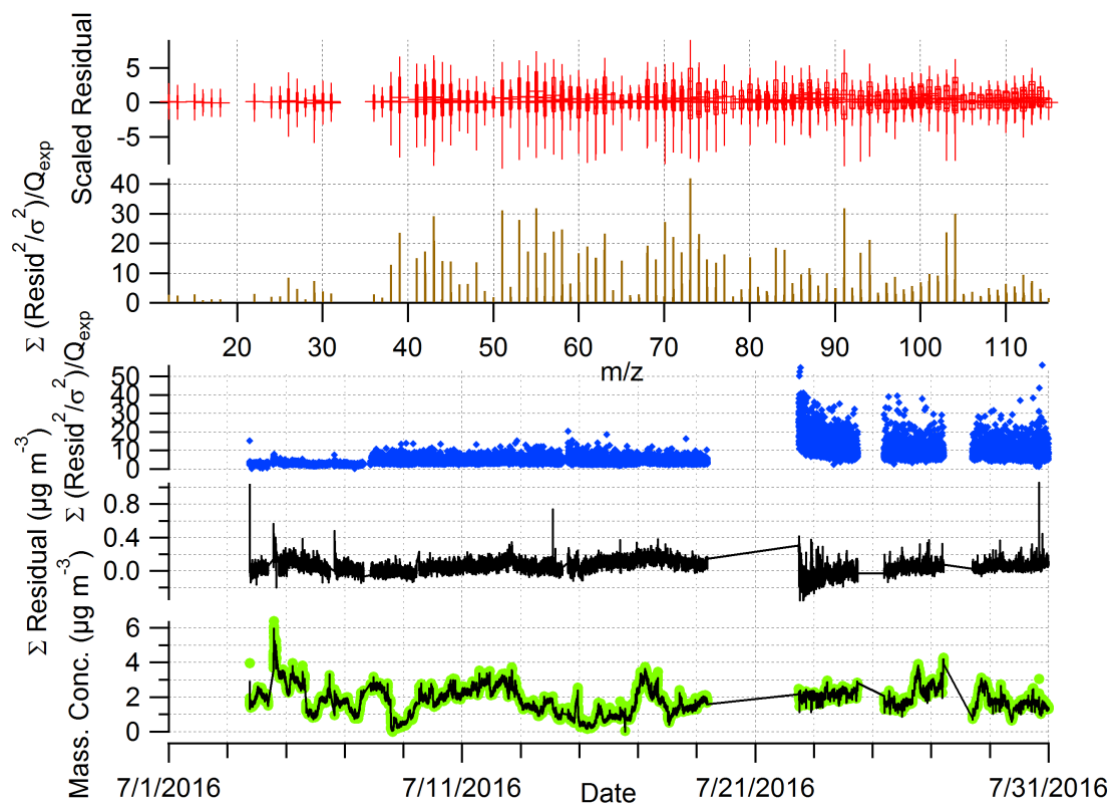


Figure S 11: Model residual diagnostic plots for the three-factor solution resolved for above-canopy OA data, from top to bottom, respectively: box and whisker plot of the scaled residuals for each m/z where boxes represent $\pm 25\%$ of points, Q/Q_{exp} contribution for each m/z , Q/Q_{exp} contribution for each time step, residuals (=measured – reconstructed) of the least-squares-fit for each time step, time series of the measured and reconstructed organic mass. An AMS power supply and pump failure event occurred on 7/19 leading to an instrument breakdown. The subsequent pumping down effect of the AMS and instrumental issues (i.e., mass spectrometer tuning) leads to increases in PMF model residuals between 7/22 and 7/31, as shown in the Q/Q_{exp} contribution for each time step panel. The effects from AMS power supply failures on increases in PMF model residuals has been observed in other studies (Crippa et al., 2013; Mohr et al., 2012).

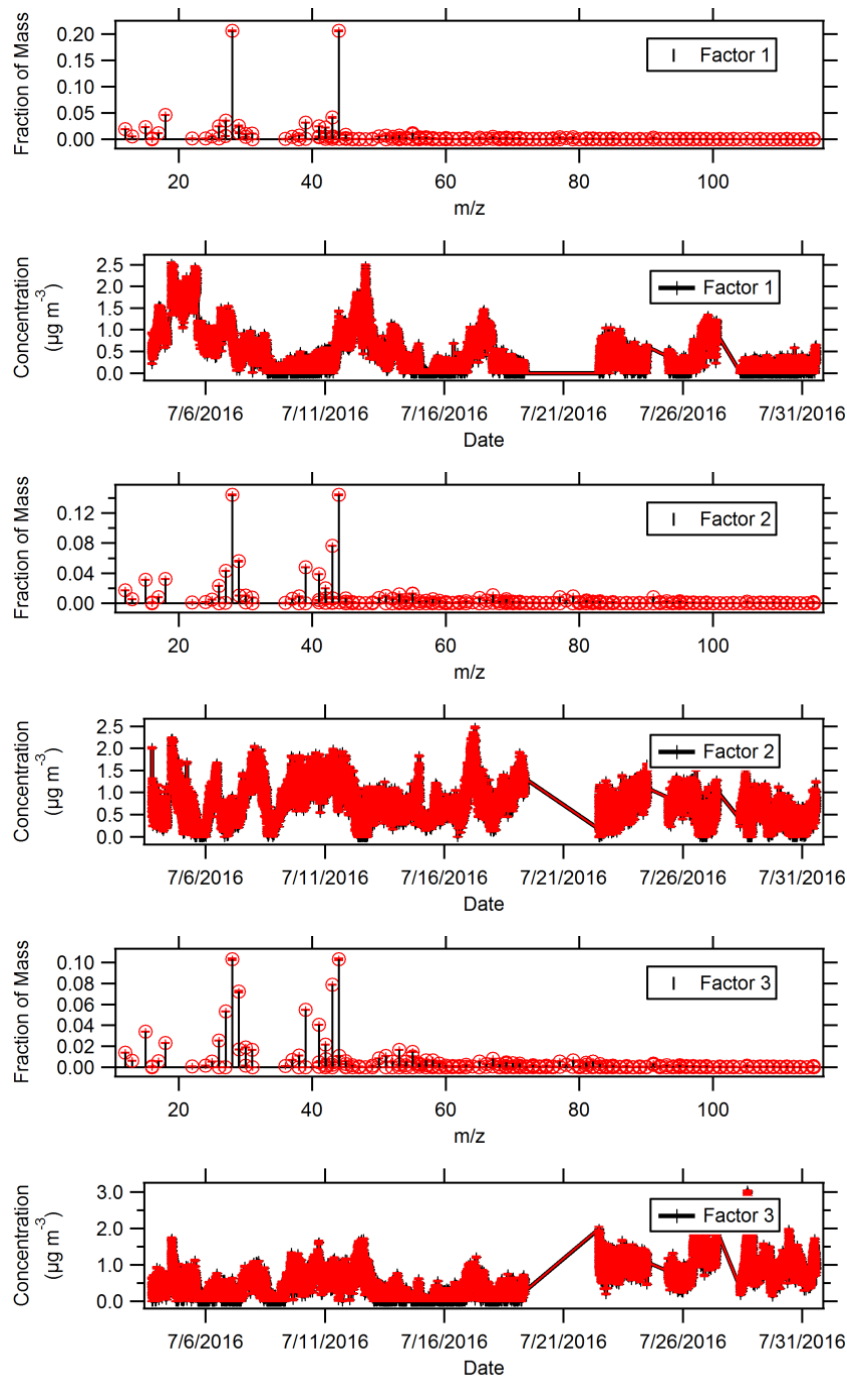


Figure S 12: Average mass spectra and time series of above-canopy OA for 100 bootstrapping runs for the three-factor solution from top to bottom, respectively: Factor 1 (MO-OOA), Factor 2 (91Fac), and Factor 3 (IEPOX-OA), where averages are shown in black and one standard deviation from the mean is shown in red.

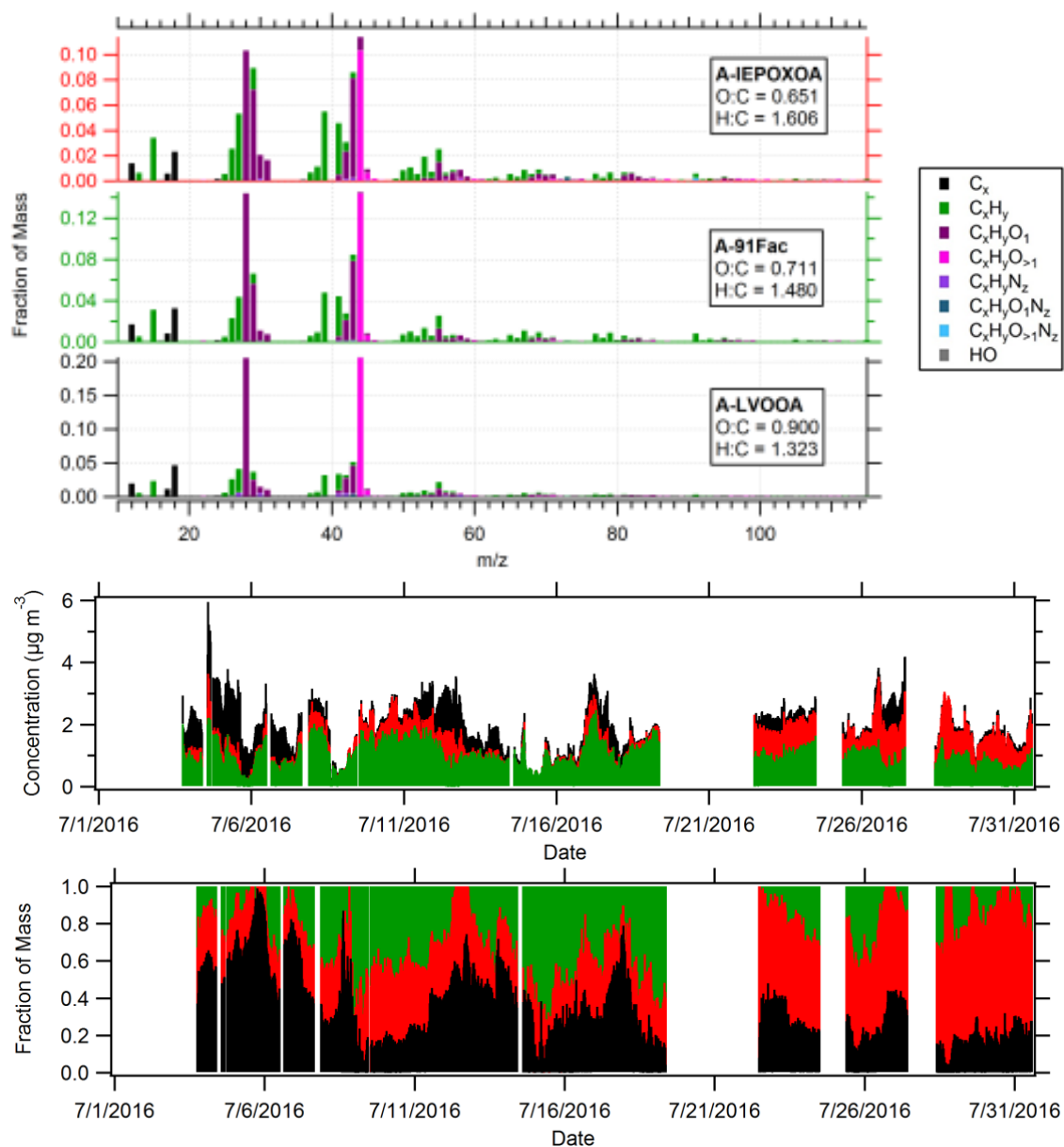


Figure S 13: (top) High-resolution mass spectra, (middle) time series of OA factor mass concentrations, and (bottom) time series of fractional contributions of OA factors to total OA for the optimal three-factor solution resolved for above-canopy OA during the PROPHET-AMOS campaign. High-resolution mass spectra are colored by their ion families, as shown in the legend of the top panel.

1 Below-canopy PMF solution

2 Table S 10 summarizes the PMF factor selection for the below-canopy OA data. Table S 11 presents time series
3 correlations with external data for different PMF factor solutions. Table S 12 presents factor mass spectra correlations with
4 reference mass spectra for different PMF solutions.

5 A one-factor solution results in an OOA. However, inspection of the time series of the measured and reconstructed
6 OA mass and the time series of total residuals indicates periods where the model does not properly fit the temporal variation
7 of OA. Factor time series and mass spectra are shown for the two-factor, three-factor, four-factor, and five-factor solution in
8 Figure S 14, Figure S 15, Figure S 16, and Figure S 17, respectively.

9 A two-factor solution (Figure S 14) reduces Q/Q_{exp} from the one-factor solution by approximately 0.143 (4%
10 decrease) (as shown in Q/Q_{exp} values in Table S 10. This solution yields two factors (MO-OOA and LO-OOA) with
11 distinct time series. Similar to the above-canopy PMF solution, the MO-OOA factor correlates with AVOCs (i.e., benzene,
12 C_3 -benzenes, C_4 -benzenes, and toluene; $R > 0.4$), SO_4 ($R > 0.72$), and NH_4 ($R > 0.76$), while the LO-OOA correlates most
13 strongly ($R = 0.56$) with the fC5H6O AMS tracer.

14 Increasing the number of factors to three (Figure S 15) yields one MO-OOA and two LO-OOAs with distinct and
15 time series. This solution reduces Q/Q_{exp} by approximately 0.07 (2% decrease from the two-factor solution). Similar to the
16 above-canopy PMF three-factor solution, the addition of this new factor (Factor 3/LO-OOA) introduces moderate
17 correlations ($R > 0.4$) with multiple unidentified terpene oxidation products. Unidentified VOCs are described in Table S 7,
18 and the below-canopy time series correlations with these VOCs are shown in Table S 13.

19 Further increasing the number of factors to four (Figure S 16) yields one MO-OOA and three LO-OOAs. However,
20 the noise in the time series of the additional factor (LO-OOA/Factor 4) indicates that this factor is not physically meaningful.
21 For the five-factor solution (Figure S 17), one MO-OOA, three LO-OOAs, and an unidentified factor with mass spectra
22 similar to IEPOX-OA ($R = 0.93$) and a distinct peak at m/z 82 are resolved. Correlations amongst the mass spectra of the
23 additional factor (Factor 5) indicate strong correlations between Factor 5 and Factors 1-4 ($R > 0.9$), as shown in Figure S 18.
24 Meanwhile, correlations of the mass spectra between factors 1-4 are weakened. Taken together, these factor correlation
25 trends indicate evidence of factor splitting. The five-factor solution also yields an unrealistic factor (Factor 2/MO-OOA)
26 with signal dominated by m/z 29 and m/z 44 ($> 45\%$ of the factor mass spectra). Furthermore, the additional factors
27 encountered in the four- and five-factor solutions cannot be justified based on correlations with any separate and external
28 data. PMF solutions with numbers of factors greater than five yield additional factors that are not physically meaningful.
29 Additionally, as shown in Figure S 18 in a four-factor solution, the correlation of the time series and mass spectra between
30 factors indicates that the mass spectra of Factor 4 is similar to Factors 1-3 ($R = 0.8 - 1.0$). Specifically, the correlation of
31 Factor 3 and Factor 4 mass spectra is $R = 0.99$. This is evidence of factor splitting. A weakening of time series correlations
32 between factors and unidentified terpene oxidation products is also observed (Table S 13). Therefore, the three-factor
33 solution is the optimal solution that is chosen for the below-canopy OA data.

34 Figure S 19 displays the diagnostic plots for the three-factor solution by varying FPEAK and SEED. To investigate
35 the effects of local minima on the three-factor solution, the PMF model was initialized at 50 different SEEDS in increments
36 of 1. Figure S 19 indicates that values for Q/Q_{exp} (top right panel) and the mass fraction of the factors (middle panel) do not
37 change across SEEDS. The rotational ambiguity of the mass spectra is analyzed by changing the FPEAK parameter between
38 -1.0 and 1.0 in increments of 0.2. Changing FPEAK indicates that the Q/Q_{exp} does not change significantly between -1.0
39 and 1.0. The maximum change in Q/Q_{exp} across FPEAK values is 0.07%. Table S 14 presents the results of the FPEAK
40 analysis where correlations with reference mass spectra are shown with the three-factor solution at different FPEAK values.
41 Correlations of the three-factor solution mass spectra with reference mass spectra do not change significantly between
42 FPEAK = 0 and FPEAK < 0.0 (Table S 12 for FPEAK = 0 and Table S 14 for FPEAK < 0.0). However, at FPEAK = + 0.2,
43 it should be noted that an increase in correlation with reference mass spectra compared to the FPEAK = 0 solution (2-5%

increase) is observed. For instance, the correlation between Factor 2 and a reference mass spectra for IEPOX-OA from Hu et al. (2015) increases from $R = 0.94$ at $FPEAK = 0$ (Table S 12) to $R = 0.98$ at $FPEAK = +0.2$ (Table S 14). Additionally, it should be noted that time series correlations between Factor 3 and unidentified VOC mass 139 (Table S 13) increases from $R = 0.47$ to $R = 0.60$ for $FPEAK = 0$ to $FPEAK = +0.2$, respectively. Similarly, correlations increase from $R = 0.48$ to $R = 0.54$ for mass 169, and from $R = 0.06$ to $R = 0.31$ for mass 113. However, no improvement in the time series or mass spectra of model residuals is observed across different $FPEAK$ values to justify a $FPEAK = +0.2$ selection. Table S 15 provides a comparison of the mass spectra between the optimal above-canopy PMF solution and the below-canopy PMF solution at $FPEAK = -0.2, 0.0$, and $+0.2$. Results indicate that the mass spectra from above- and below-canopy OA at $FPEAK = 0.0$ are identical ($R = 1.0$). Therefore, the $FPEAK$ analysis indicates that $FPEAK = 0$ is the appropriate solution for below-canopy OA. Figure S 20 shows the model diagnostic plots for time series and mass spectra residuals for the optimal three-factor solution ($FPEAK = 0$ and $SEED = 0$).

Results from 100 bootstrapping runs of the optimal three-factor solution at $SEED = 0$ and $FPEAK = 0$ are shown in Figure S 21. Bootstrapping analysis indicate that the uncertainties of the time series and mass spectra of all factors are small in comparison to the time series and mass spectra signals. This indicates a robust solution over 100 bootstrapping runs. For instance, the standard deviation for the mass fraction of CO_2^+ ion (m/z 43.98) in the Factor 1 mass spectra is $< 0.5\%$ of the average CO_2^+ mass fraction. The high-resolution mass spectra, time series of factor mass concentrations, and time series of fractional contributions of OA factors to total OA for the optimal below-canopy OA solution is shown in Figure S 22.

1 Table S 10: Summary of PMF factor selection for below-canopy OA data.

# Factors	FPEAK	SEED	$Q/Q_{expected}$	$\Delta Q/Q_{expected}^1$	Solution Description
2	0	0	3.97729	-0.14314	Two-factor solution
3	0	0 to 50 in steps of 1	3.90198 – 3.90201	---	Three-factor solution is stable across seeds, so SEED = 0 is chosen.
3	-1.0 to 1.0 in increments of 0.2	0	3.90458 – 3.90199	---	Three-factor solution across FPEAKs indicates similar mass spectra, so FPEAK = 0 is chosen.
3	0	0	3.90198	-0.07531	Optimal three-factor solution yields factors with distinct time series and correlations with external time series and mass spectra data.
4	0	0	3.85334	-0.04864	Noisy time series of additional factor and strongly correlated mass spectra of the four-factors ($R > 0.8$).
5	0	0	3.81417	-0.03917	Noisy time series of additional factor and strongly correlated mass spectra of five-factor solution ($R > 0.9$).
6 to 8	0	0	3.78501 to 3.73390	-0.02916 to -0.0244	For solutions greater than the five-factors, no strong change in the slope of Q/Q_{exp} is observed and physically meaningless factors are extracted.

2 ¹This value represents the difference between the Q/Q_{exp} (P) and Q/Q_{exp} (P-1) factor solution, where P = # of factors
3

1 **Table S 11: Summary of different PMF factor solutions for below-canopy OA data and time series correlations with external data. Table entries shaded**
2 **in gray represent correlation coefficients that are greater than or equal to 0.40.**

	Two-factor		Three-factor			Four-factor				Five-factor				
	VOCs ^a , R _{Time Series}													
Factor #	1	2	1	2	3	1	2	3	4	1	2	3	4	5
Acetaldehyde	0.21	0.15	0.25	0.29	-0.10	0.24	0.28	-0.02	0.15	0.34	0.25	0.12	0.14	0.00
Acetonitrile	0.54	-0.02	0.59	0.19	-0.16	0.58	0.18	-0.07	0.11	0.21	0.59	0.12	0.09	-0.01
Acetone	0.40	-0.14	0.46	0.12	-0.30	0.45	0.09	-0.22	0.07	0.19	0.46	0.05	0.05	-0.17
Benzene	0.68	-0.10	0.66	0.04	0.00	0.66	0.03	0.02	0.09	0.15	0.64	0.36	0.08	-0.14
C ₂ -benzenes	0.36	0.08	0.29	0.01	0.26	0.29	0.03	0.22	0.09	0.05	0.27	0.34	0.09	0.03
C ₃ -benzenes	0.42	0.20	0.34	0.09	0.37	0.34	0.11	0.35	0.11	0.12	0.31	0.43	0.11	0.12
C ₄ -benzenes	0.41	0.07	0.32	-0.05	0.35	0.31	-0.03	0.28	0.08	-0.01	0.29	0.39	0.09	0.04
C ₄ -carbonyls	0.67	-0.08	0.69	0.13	-0.11	0.69	0.13	-0.04	0.08	0.26	0.68	0.33	0.06	-0.15
C ₅ -carbonyls	0.68	-0.14	0.70	0.08	-0.14	0.69	0.06	-0.09	0.09	0.18	0.68	0.27	0.07	-0.17
C ₆ -carbonyls	0.47	-0.02	0.50	0.17	-0.13	0.49	0.16	-0.06	0.11	0.25	0.49	0.18	0.10	-0.08
Isoprene	0.08	0.28	0.11	0.32	0.03	0.11	0.32	0.13	0.12	0.28	0.11	0.07	0.11	0.19
Methanol	0.28	0.03	0.33	0.19	-0.14	0.32	0.18	-0.06	0.08	0.19	0.33	0.03	0.06	0.04
Methylfuran	0.27	0.24	0.26	0.27	0.12	0.26	0.27	0.17	0.17	0.29	0.24	0.25	0.16	0.11
Monoterpenes	0.23	0.19	0.24	0.27	0.02	0.24	0.28	0.10	0.12	0.33	0.23	0.23	0.10	0.04
MVK+MACR	0.16	0.21	0.09	0.08	0.32	0.09	0.09	0.29	0.11	0.03	0.08	0.21	0.11	0.20
Toluene	0.42	0.07	0.36	0.03	0.23	0.36	0.04	0.21	0.09	0.05	0.33	0.33	0.09	0.04

	Trace Gases ^b , R _{Time Series}													
Factor #	1	2	1	2	3	1	2	3	4	1	2	3	4	5
CO	0.66	0.12	0.66	0.19	0.12	0.65	0.19	0.16	0.19	0.19	0.65	0.26	0.19	0.15
NO ₂	0.42	-0.09	0.36	-0.12	0.20	0.36	-0.12	0.14	0.02	-0.06	0.33	0.31	0.02	-0.09
NO _y	0.53	-0.17	0.49	-0.11	0.06	0.49	-0.12	0.03	0.02	-0.04	0.47	0.27	0.02	-0.13
O ₃	0.29	-0.15	0.32	0.02	-0.21	0.31	-0.00	-0.17	0.04	0.03	0.32	-0.03	0.02	-0.09
O _x	0.30	-0.13	0.33	0.02	-0.16	0.32	0.00	-0.14	0.06	0.04	0.32	0.02	0.04	-0.09

	NR-PM ₁ , R _{Time Series}													
Factor #	1	2	1	2	3	1	2	3	4	1	2	3	4	5
f _{C5H6O}	-0.52	0.56	-0.49	0.54	-0.02	-0.48	0.57	0.16	0.08	0.57	-0.47	-0.07	0.09	0.26
SO ₄	0.72	-0.13	0.78	0.15	-0.22	0.78	0.14	-0.09	0.04	0.25	0.78	0.24	0.03	-0.09
NH ₄	0.76	-0.16	0.82	0.10	-0.20	0.82	0.09	-0.09	0.04	0.18	0.82	0.21	0.03	-0.07
NO ₃	0.72	-0.06	0.71	0.02	0.11	0.71	0.02	0.13	0.07	-0.01	0.71	0.25	0.07	0.11
Chl	0.27	-0.03	0.27	0.03	0.00	0.27	0.02	0.03	0.02	0.00	0.27	0.05	0.02	0.06

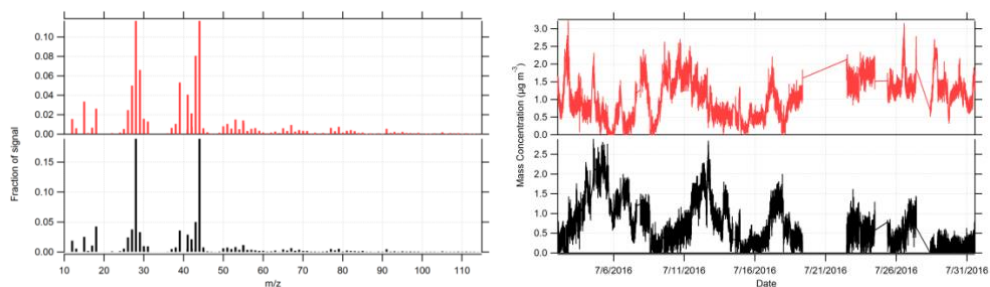
3 ^a VOCs measured using University of Minnesota's PTR-QiTOF from the 5-m inlet on the PROPHET tower.

4 ^b Trace gases measured from 6-m common inlet on the MAQL.

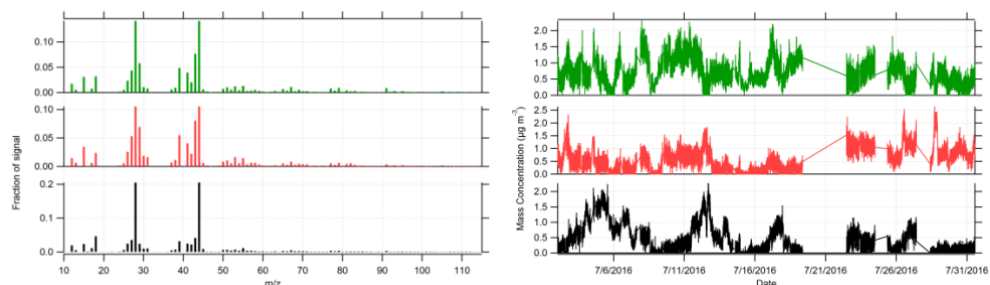
5

1 Table S 12: Summary of PMF factor solutions for below-canopy OA data and correlation coefficients with reference mass spectra
2 from the unit-mass resolution and high-resolution AMS spectral database, where table entries shaded in gray represent
3 correlation coefficients that are greater than or equal to 0.80. PMF solutions with SEED = 0 and FPEAK = 0 are shown.
4 Reference mass spectra from the unit-mass resolution and high-resolution AMS spectral database are used for comparison to the
5 below-canopy PMF factor solutions (Ulbrich et al., 2009).

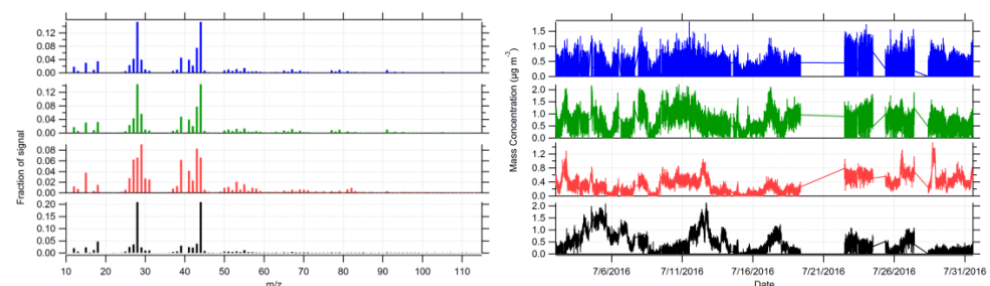
	2-factor		3-factor			4-factor				5-factor				
	<i>Reference Mass Spectra, R_{Mass Spectra}</i>													
	1	2	1	2	3	1	2	3	4	1	2	3	4	5
MO-OOA ^a	0.85	0.81	0.85	0.79	0.84	0.84	0.69	0.84	0.85	0.55	0.83	0.85	0.85	0.82
LO-OOA ^a	0.68	0.86	0.63	0.86	0.83	0.61	0.85	0.83	0.80	0.75	0.56	0.80	0.80	0.86
BBOA ^a	0.59	0.81	0.53	0.83	0.76	0.52	0.87	0.75	0.70	0.85	0.45	0.75	0.71	0.76
HOA ^a	0.34	0.52	0.29	0.53	0.49	0.28	0.54	0.49	0.47	0.49	0.23	0.47	0.47	0.51
IEPOX-OA ^b	0.74	0.88	0.70	0.88	0.85	0.69	0.87	0.85	0.81	0.79	0.63	0.84	0.81	0.85
IEPOX-OA ^c	0.73	0.92	0.69	0.94	0.86	0.68	0.98	0.85	0.82	0.93	0.63	0.85	0.81	0.87
82Fac ^d	0.55	0.67	0.53	0.68	0.63	0.52	0.72	0.63	0.62	0.69	0.50	0.61	0.61	0.67
91Fac ^d	0.70	0.84	0.66	0.84	0.82	0.64	0.82	0.81	0.80	0.74	0.59	0.81	0.80	0.82



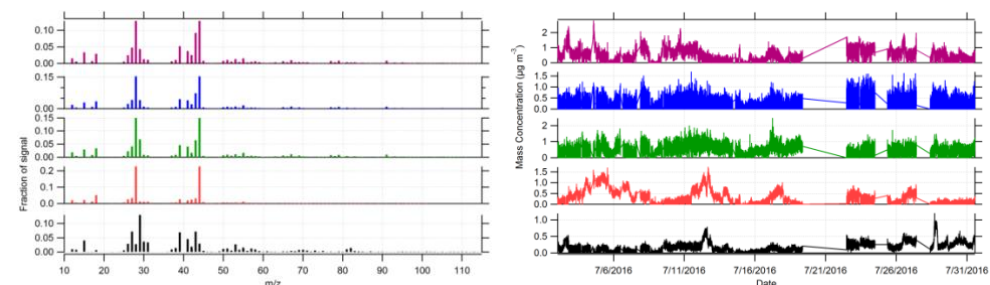
1
2 **Figure S 14: (left) Mass spectra and (right) time series for the two-factor solution for below-canopy OA, where Factor 2 and**
3 **Factor 1 are shown from top to bottom, respectively.**



4
5 **Figure S 15: (left) Mass spectra and (right) time series for the three-factor solution for below-canopy OA, where Factor 3, Factor**
6 **2, and Factor 1 are shown from top to bottom, respectively.**



7
8 **Figure S 16: (left) Mass spectra and (right) time series for the four-factor solution for below-canopy OA, where Factors 4 through**
9 **1 are shown from top to bottom, respectively.**



10
11 **Figure S 17: (left) Mass spectra and (right) time series for the five-factor solution for below-canopy OA, where Factors 5 through 1**
12 **are shown from top to bottom respectively.**

1 **Table S 13: Summary of correlation coefficients between different PMF factor solutions for below-canopy OA data and VOCs**
2 **measured by University of Minnesota's PTR-QiTOF. Further information regarding unidentified VOCs can be found in Table S**
3 **7. Table entries shaded in gray represent correlation coefficients that are greater than or equal to 0.40. PMF solutions with SEED**
4 **= 0 and FPEAK = 0 are shown.**

Two-factor			Three-factor			Four-factor				Five-factor				
VOCs Masses from Table S 7, R Time Series														
Factor #	1	2	1	2	3	1	2	3	4	1	2	3	4	5
47.011	0.30	0.23	0.34	0.32	-0.01	0.34	0.32	0.11	0.14	0.21	0.35	-0.04	0.13	0.33
47.0478	0.08	0.05	0.08	0.07	0.01	0.08	0.07	0.04	0.03	0.10	0.08	0.11	0.03	-0.02
57.034	0.47	0.19	0.49	0.28	0.04	0.49	0.28	0.15	0.15	0.25	0.49	0.16	0.14	0.22
61.029	0.43	0.27	0.48	0.41	-0.04	0.47	0.40	0.10	0.22	0.34	0.49	0.06	0.21	0.29
73.02691	0.45	0.31	0.47	0.40	0.06	0.47	0.40	0.17	0.25	0.38	0.47	0.19	0.24	0.24
75.0446	0.58	0.04	0.59	0.14	0.04	0.59	0.15	0.14	0.03	0.06	0.60	0.10	0.02	0.24
113.05511	0.29	0.43	0.33	0.51	0.06	0.32	0.51	0.19	0.28	0.45	0.33	0.11	0.27	0.34
115.07355	0.63	0.15	0.64	0.26	0.06	0.64	0.26	0.15	0.19	0.24	0.64	0.23	0.18	0.18
127.07339	0.39	0.37	0.39	0.35	0.24	0.38	0.36	0.31	0.23	0.28	0.38	0.21	0.22	0.35
127.10961	0.43	0.21	0.42	0.23	0.18	0.41	0.23	0.22	0.19	0.20	0.41	0.23	0.18	0.20
129.08796	0.58	0.21	0.56	0.23	0.22	0.56	0.24	0.27	0.20	0.20	0.55	0.30	0.19	0.23
139.11197	0.11	0.51	0.06	0.32	0.47	0.05	0.34	0.48	0.23	0.26	0.04	0.29	0.23	0.38
151.11044	0.33	0.19	0.25	0.04	0.43	0.25	0.05	0.36	0.13	0.01	0.23	0.34	0.13	0.18
169.12196	0.26	0.36	0.19	0.18	0.48	0.19	0.20	0.45	0.18	0.14	0.17	0.34	0.18	0.30
205.1956	0.12	0.20	0.07	0.07	0.32	0.07	0.08	0.26	0.12	0.07	0.06	0.25	0.12	0.11
237.18584	0.29	0.08	0.26	0.02	0.22	0.25	0.03	0.20	0.06	0.01	0.24	0.21	0.06	0.11
253.1774	0.18	0.10	0.17	0.09	0.10	0.17	0.09	0.12	0.06	0.08	0.17	0.12	0.05	0.10

5

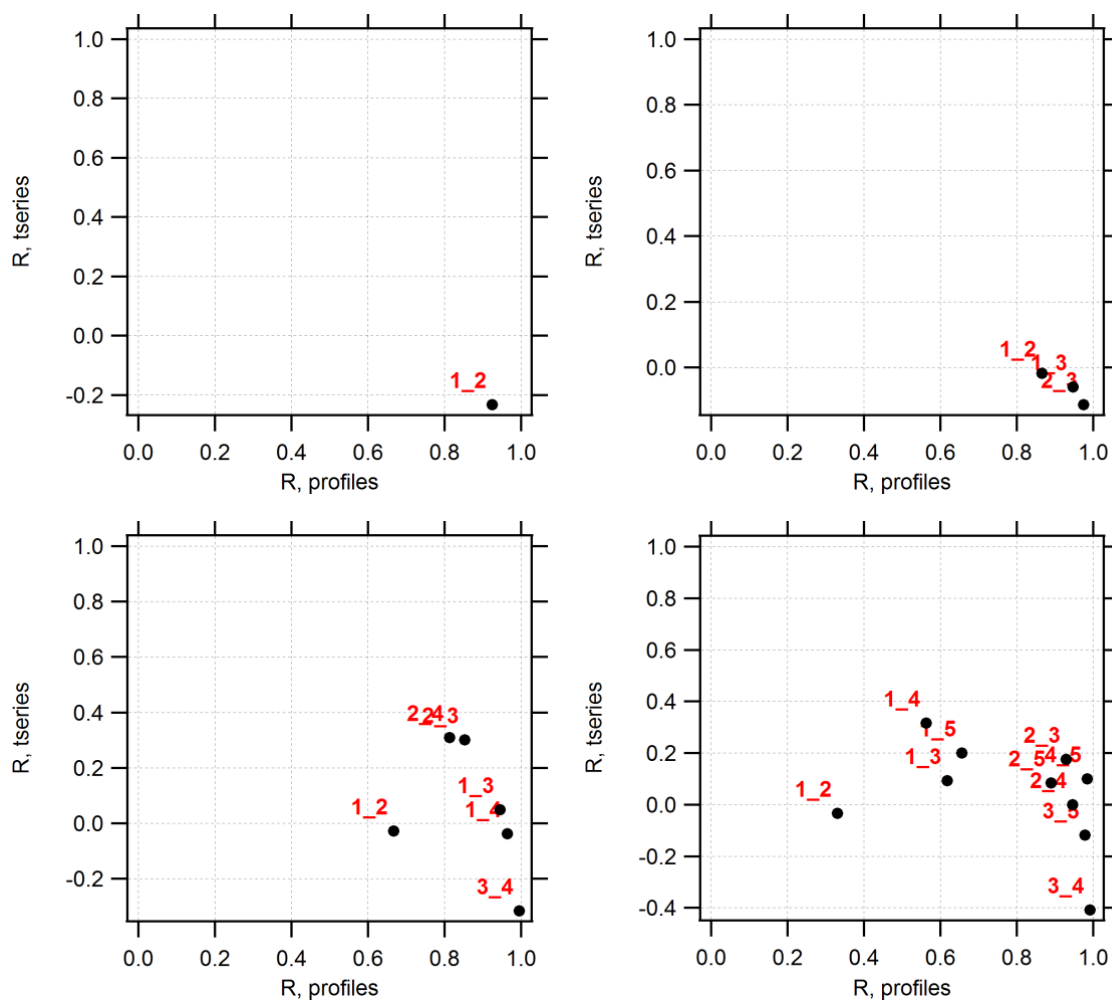
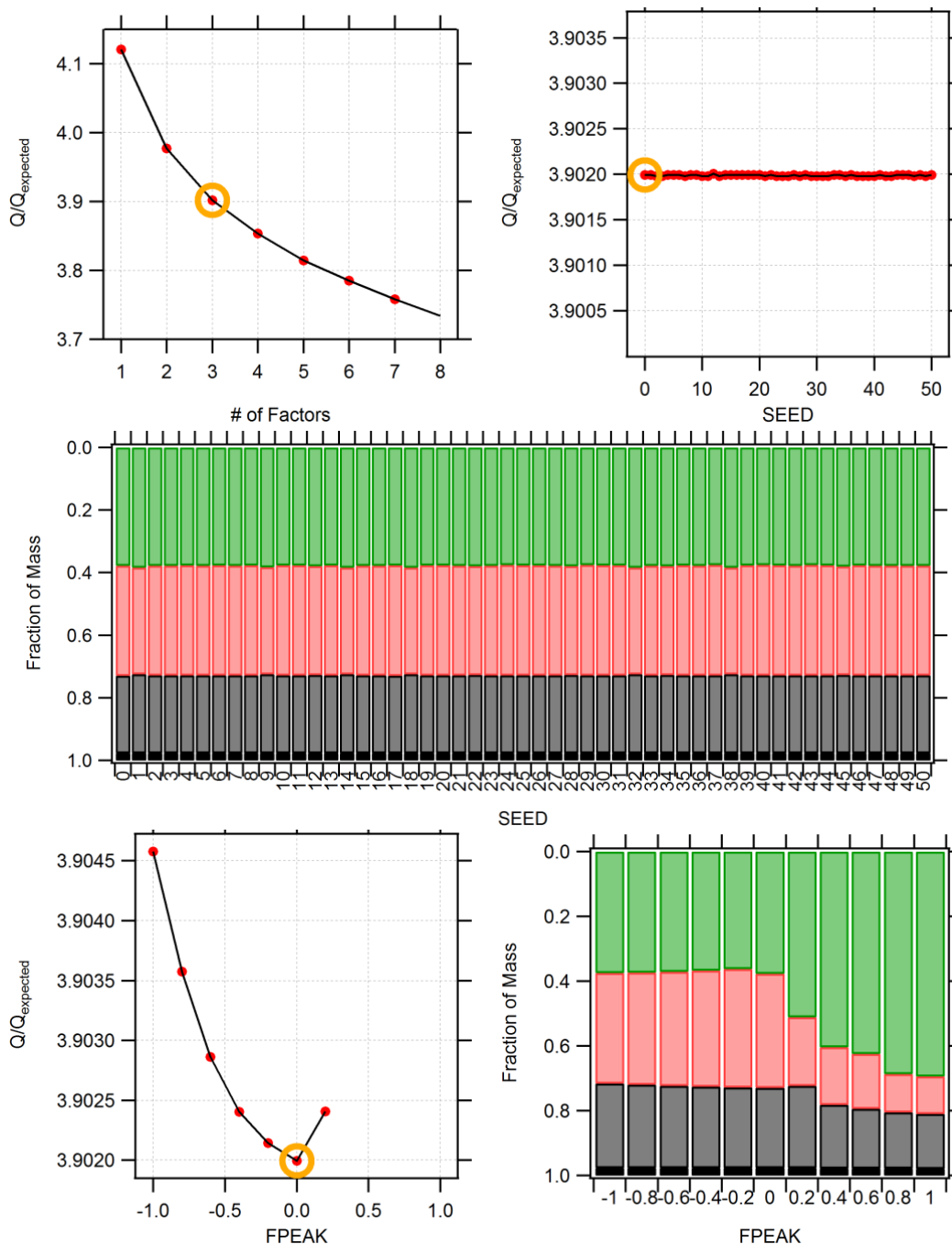


Figure S 18: Factor correlation coefficient plots based on factor time series (“R, tseries”) and factor mass spectra (“R, profiles”) of below-canopy OA data for the following: (top left) two-factor solution, (top right) three-factor solution, (bottom left) four-factor solution, and (bottom right) five-factor solution. Correlation coefficients are shown with black circles, and are labeled as $R_{i,j}$, where i and j represent the factor numbers i and j within a given PMF solution.



1

2

3

4 **Figure S 19: Q/Q_{exp} , SEED, and FPEAK related diagnostic plots for three-factor solution resolved for below-canopy OA: (top left)**
5 **Q/Q_{exp} vs. number of factors, (top right) Q/Q_{exp} vs. SEED ranging from 1 to 50 in increments of 1, (middle) mass fraction of PMF**
6 **factors vs. SEED, (bottom left) Q/Q_{exp} vs. FPEAK ranging from -1.0 to +0.2 in increments of 0.2, and (bottom right) mass fraction**
7 **of PMF factors vs. FPEAK. The orange circle denotes the chosen PMF solution. Values of Q/Q_{exp} are not shown for solutions with**
8 **FPEAK > +0.2 because solutions with FPEAK > +0.2 did not converge.**

1 **Table S 14: Summary of correlation coefficients of the three-factor PMF solution for below-canopy OA data with reference mass**
2 **spectra using FPEAK analysis, where FPEAK ranges from -1.0 to +0.2 in increments of 0.2. PMF solutions with FPEAK values**
3 **greater than 0.2 did not achieve convergence, and are not shown. Reference mass spectra from the unit-mass resolution and high-**
4 **resolution AMS spectral database are used for comparison to the below-canopy PMF factor solutions at different FPEAK values**
5 **(Ulbrich et al., 2009).**

FPEAK	-1.0			-0.8			-0.6		
	1	2	3	1	2	3	1	2	3
MO-OOA^a	0.85	0.84	0.80	0.85	0.84	0.80	0.85	0.84	0.80
LO-OOA^a	0.66	0.82	0.86	0.65	0.82	0.86	0.64	0.83	0.86
BBOA^a	0.57	0.75	0.82	0.56	0.75	0.82	0.55	0.76	0.82
HOA^a	0.32	0.48	0.52	0.31	0.48	0.52	0.31	0.48	0.52
IEPOX-OA^b	0.72	0.85	0.88	0.72	0.85	0.88	0.71	0.85	0.88
IEPOX-OA^c	0.72	0.86	0.93	0.71	0.86	0.93	0.70	0.86	0.93
82Fac^d	0.54	0.63	0.67	0.54	0.63	0.67	0.53	0.63	0.67
91Fac^d	0.68	0.81	0.84	0.68	0.81	0.84	0.67	0.81	0.84
FPEAK	-0.4			-0.2			+0.2		
	1	2	3	1	2	3	1	2	3
MO-OOA^a	0.85	0.84	0.80	0.85	0.84	0.79	0.85	0.74	0.84
LO-OOA^a	0.64	0.83	0.86	0.63	0.83	0.86	0.63	0.86	0.83
BBOA^a	0.54	0.76	0.83	0.54	0.76	0.83	0.53	0.86	0.76
HOA^a	0.30	0.48	0.53	0.30	0.49	0.53	0.29	0.54	0.49
IEPOX-OA^b	0.70	0.85	0.88	0.70	0.85	0.88	0.70	0.88	0.85
IEPOX-OA^c	0.70	0.86	0.94	0.69	0.86	0.94	0.69	0.98	0.86
82Fac^d	0.53	0.63	0.68	0.53	0.63	0.68	0.53	0.71	0.63
91Fac^d	0.66	0.81	0.84	0.66	0.82	0.84	0.66	0.84	0.82

6 ^a Average MS from multiple ambient data sets (Ng et al., 2011).

7 ^b Atlanta, GA in Summer 2011, Source: (Budisulistiorini et al., 2013).

8 ^c Southern Oxidant and Aerosol Study (SOAS) in Centreville, AL in Summer 2013 (Hu et al., 2015).

9 ^d Malaysian Borneo rainforest in 2008 (Robinson et al., 2011a).

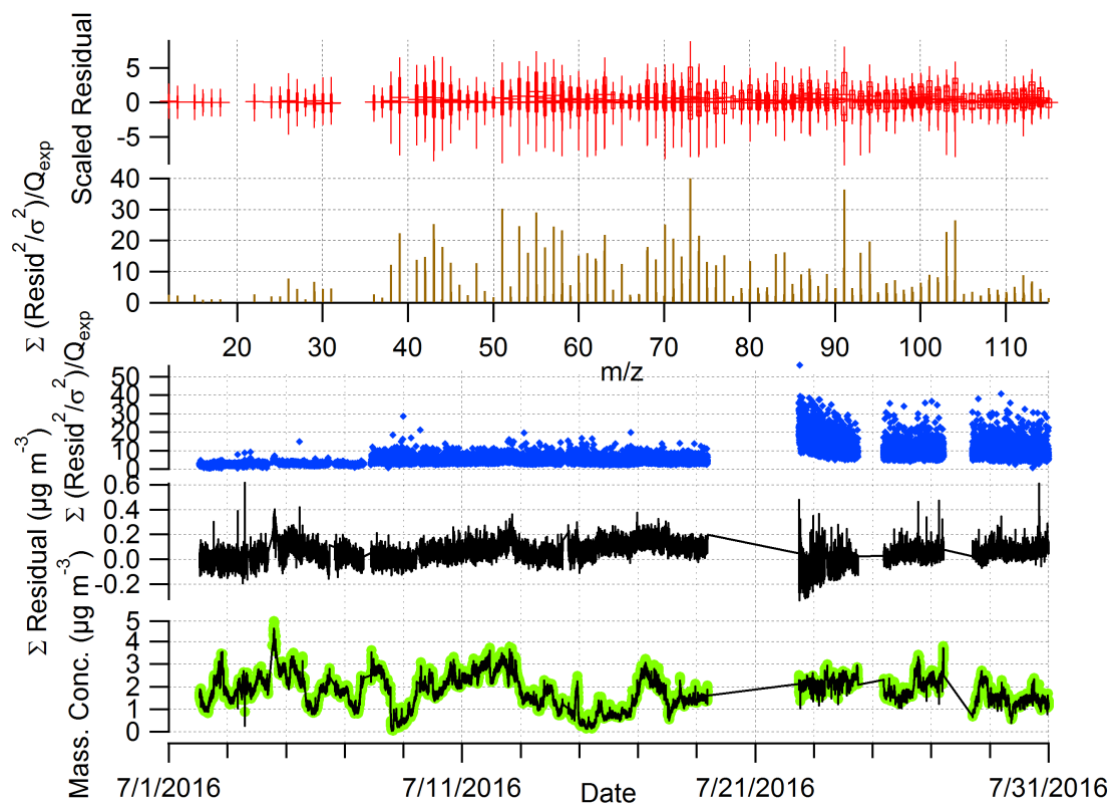
10

11 **Table S 15: Correlations of above-canopy and below-canopy three-factor solutions across -0.2 and +0.2 FPEAK values for below-**
12 **canopy OA.**

Below-Canopy OA PMF solutions @ FPEAK value									
Above-Canopy OA	-0.2			0.0^a			+0.2		
	1	2	3	1	2	3	1	2	3
MO-OOA	1.00	0.95	0.88	1.00	0.87	0.95	1.00	0.79	0.95
91Fac	0.96	1.00	0.98	0.96	0.97	1.00	0.96	0.93	1.00
IEPOX-OA	0.87	0.97	1.00	0.87	1.00	0.97	0.87	0.99	0.97

13 ^a Factors 1, 2, and 3 for FPEAK = 0.0 correspond to below-canopy MO-OOA, IEPOX-OA, and 91Fac, respectively.

14



1

2 **Figure S 20: Model residual diagnostic plots for three-factor solution resolved for below-canopy OA, from top to bottom,**
3 **respectively: box and whisker plot of the scaled residuals for each m/z where boxes represent +/- 25% of points, Q/Q_{exp}**
4 **contribution for each m/z, Q/Q_{exp} contribution for each time step, residuals (=measured – reconstructed) of the least-squares-fit**
5 **for each time step, time series of the measured and reconstructed organic mass. The increases in PMF model residuals in Q/Q_{exp}**
6 **contribution time series between 7/21 and 7/31 are discussed in caption of Figure S 11.**

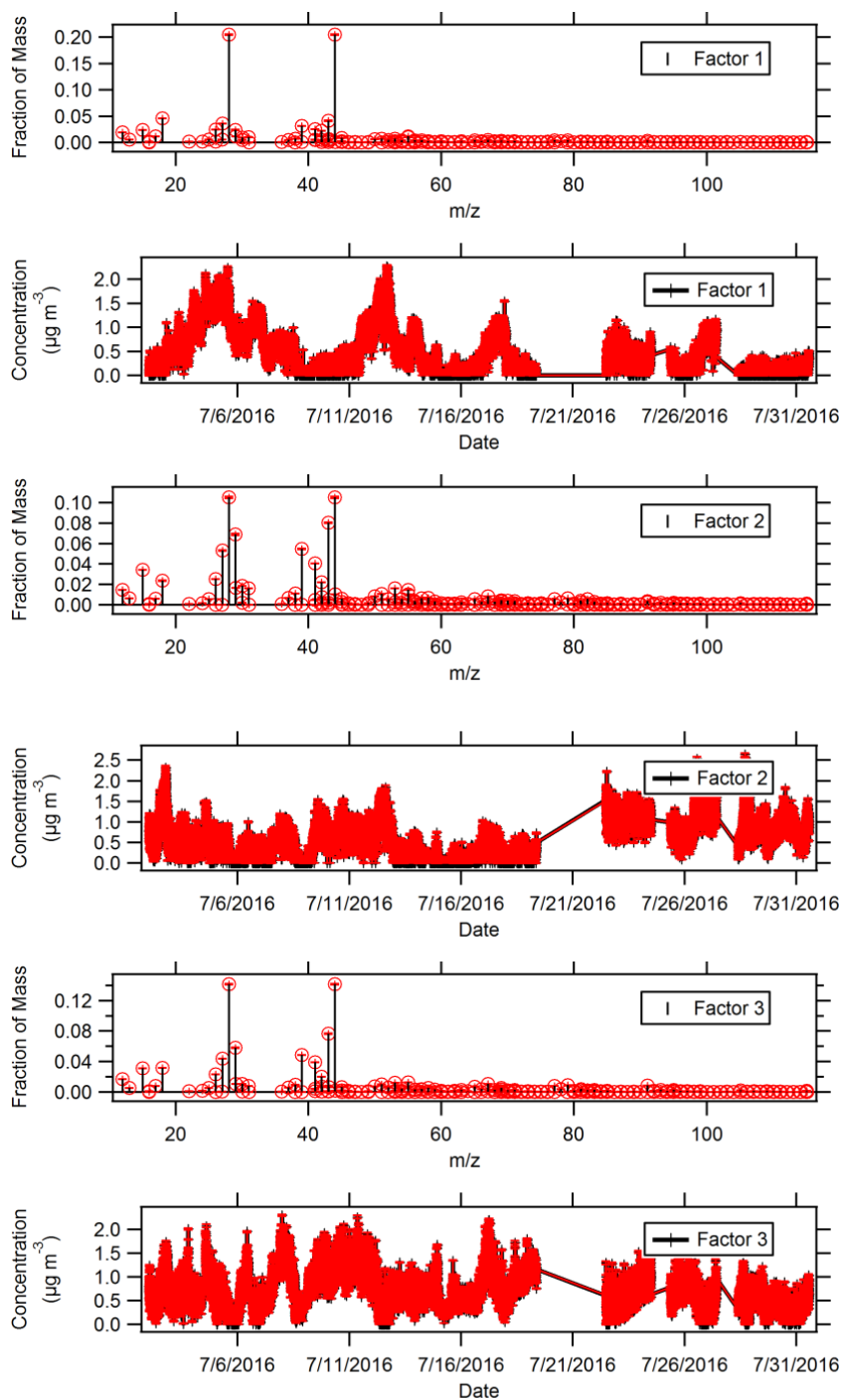


Figure S 21: Average mass spectra and time series of below-canopy OA composition for 100 bootstrapping runs for the three-factor solution from top to bottom, respectively: MO-OOA (Factor 1), IEPOX-OA (Factor 2), and 91Fac (Factor 3), where averages are shown in black and one standard deviation from the mean is shown in red.

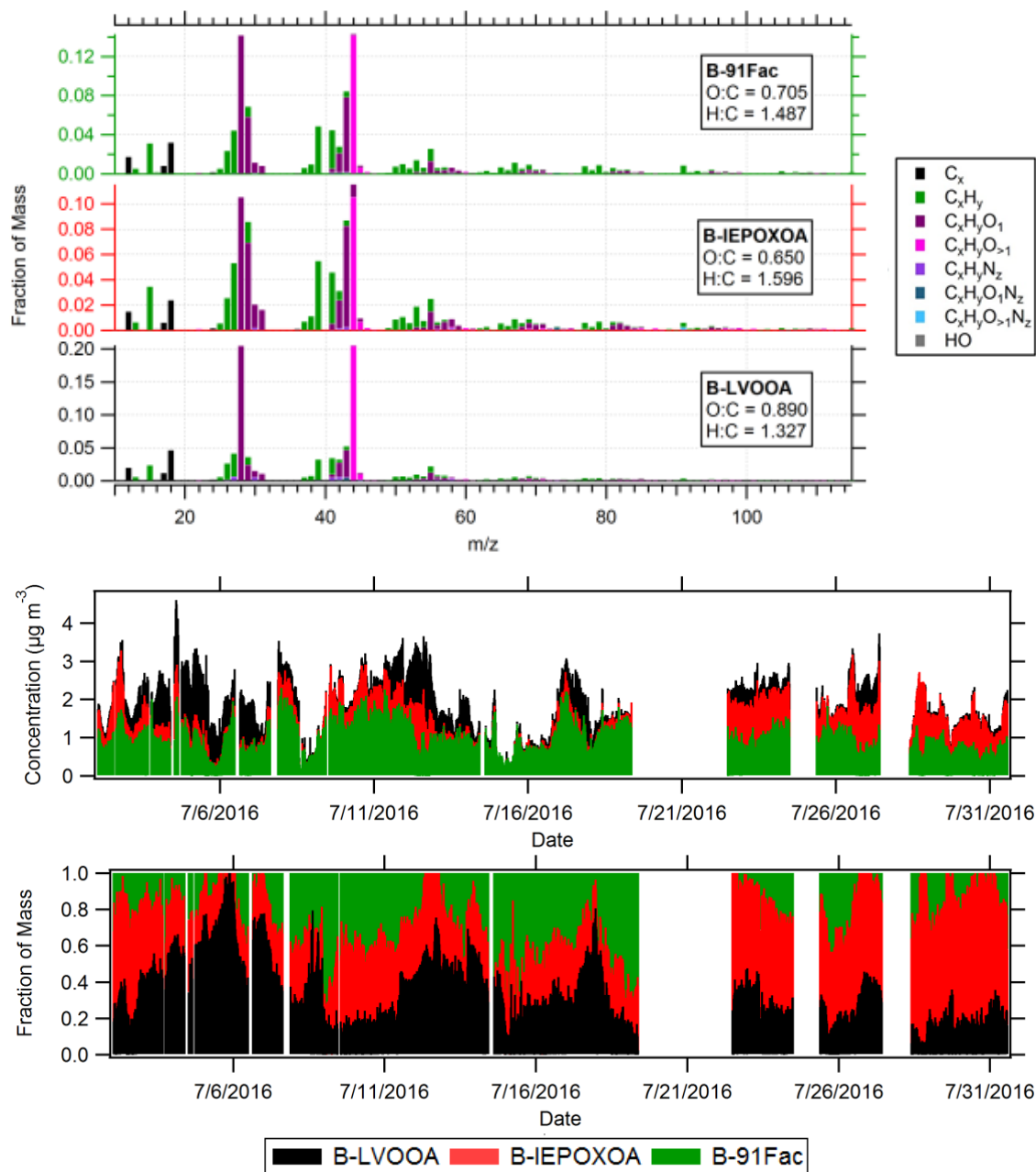


Figure S 22: (top) High-resolution mass spectra, (middle) time series of OA factor mass concentrations, and (bottom) time series of fractional contributions of OA factors to total OA for the optimal three-factor solution resolved for below-canopy OA during the PROPHET-AMOS campaign. High-resolution mass spectra are colored by their ion families, as shown in the legend of the top panel.

1 Factor description for above- and below-canopy OA

2 As discussed above, optimal three-factor solutions were resolved for both the above- and below-canopy OA
3 datasets. In the following section, characteristics of the above-canopy MO-OOA (A-MO-OOA), IEPOX-OA (A-IEPOX-
4 OA), and 91Fac (A-91Fac) and below-canopy MO-OOA (B-MO-OOA), IEPOX-OA (B-IEPOX-OA), and 91Fac (B-91Fac)
5 will be described.

6 More-oxidized oxygenated organic aerosol (MO-OOA)

7 MO-OOA is a factor that has been resolved in a number of urban, forested, and remote field studies (Jimenez et al.,
8 2009; Ng et al., 2010). In the region surrounding the PROPHET site, MO-OOA has been resolved in studies conducted in
9 Ontario, Canada, specifically in Bear Creek, Harrow, and Egbert (as OOA-1 in (Slowik et al., 2011, 2010)). MO-OOA is the
10 most oxidized factor ($O:C = 0.89\text{--}0.90$) and represents 23.4% and 23.5% of the total OA mass for the above- and below-
11 canopy OA, respectively. This OOA factor is distinguished by a prominent signal at m/z 44 ($f_{44,above} = 0.21$, $f_{44,below} = 0.20$)
12 and m/z 28 ($f_{28,above} = 0.20$, $f_{28,below} = 0.19$), and relatively lower signal at $m/z > 50$. The f_{44} of this MO-OOA factor is the
13 highest among the resolved PMF factors. A majority of the signal at m/z 44 is attributed to the CO_2^+ ion (~99% mass
14 contribution at m/z 44 for above and below the canopy). Oxygen-containing ion families, such as the $C_xH_yO_{>1}$ and $C_xH_yO_1$
15 ion families, contribute ~60% to the total mass of the MO-OOA factor.

16 A-MO-OOA and B-MO-OOA are correlated with aerosol SO_4 ($R = 0.72$), NH_4 ($R = 0.77\text{--}0.76$), and NO_3 ($R = 0.73\text{--}$
17 0.72). Highly-oxygenated OA that has been identified in previous studies (also referred to as MO-OOA, LV-OOA, or OOA-
18 1) has been shown to correlate with aerosol SO_4 and is representative of a more regional, transported OA factor (Lanz et al.,
19 2007; Slowik et al., 2010; Ulbrich et al., 2009). A-MO-OOA and B-MO-OOA are also correlated with a number of VOC
20 measurements, as shown in the PMF factor time series correlation summaries in Table S 5 and Table S 11. Correlation with
21 benzene (C_6H_6) ($R = 0.66\text{--}0.67$) indicates that MO-OOA was formed in or passed over regions impacted by anthropogenic
22 activities. Previous studies in metropolitan Paris found significant correlations between MO-OOA and benzene, which
23 suggested the influence of continental/anthropogenic emissions on MO-OOA (Crippa et al., 2013). Furthermore, at a rural
24 site in Canada (approx. 250 miles ESE from the site), Rupakheti et al. (2005) found that air masses originating from
25 urban/industrial regions from the southwest contained higher f_{44} (more OOA) and longer-lived non-methane hydrocarbons
26 (NMHCs) such as ethane and propane (lifetime of benzene with respect to OH oxidation = 10 days, (Atkinson et al., 2004)),
27 which is consistent with the associations of benzene and MO-OOA factors (highest f_{44}) resolved at this site.

28 Correlations between A-MO-OOA and B-MO-OOA and oxygenated VOCs (OVOCs: acetone (C_3H_6O , $R = 0.46\text{--}$
29 0.60), acetaldehyde (C_2H_4O , $R = 0.25\text{--}0.45$), methanol (C_2H_4O , $R = 0.33\text{--}0.51$), C_4 -carbonyls, C_5 -carbonyls, and C_6 -
30 carbonyls) suggests the similar sources of MO-OOA and these OVOCs. Correlations of MO-OOA with OVOCs that are
31 associated with long-range transported air masses further suggest the transported nature of this factor. In this region, the
32 associations of MO-OOA with acetone and particulate SO_4 is in agreement with MO-OOA resolved in previous studies in
33 the Ontario region of Canada (Slowik et al., 2011, 2010; Vlasenko et al., 2009). Finally, the A-MO-OOA and B-MO-OOA
34 mass spectra resemble reference mass spectra of MO-OOA ($R = 0.85$, as shown in Table S 6 and Table S 12, respectively).

35 The diurnal pattern for MO-OOA (Figure 3 in the main text) is relatively flat with increases during the nighttime
36 hours. This type of diurnal pattern is in contrast to MO-OOA resulting from daytime photochemical production, which
37 exhibits maximums in the afternoon, as observed in other studies in forested environments (Hao et al., 2014; Raatikainen et
38 al., 2010; Xu et al., 2015a). Multiple factors likely contribute to this type of diurnal variation, such as boundary layer
39 dynamics and long-range transport. Nighttime accumulation of MO-OOA in the shallow nocturnal boundary layer could
40 help to explain the observed increases in nighttime MO-OOA at this site. Additionally, the diurnal wind speed and wind
41 direction (Figure S 2) indicate that southwesterly winds (~240°) occurred during nighttime hours, which supports the
42 observations of MO-OOA formed from or passed over anthropogenic activities from southwest of the site during these time

1 periods. Lastly, the two MO-OOA related events (7/3-7/6 and 7/11-7/14) are mainly attributed to southerly air masses
2 (Cluster#1 in Figure S 23) using the HYSPLIT backward-trajectories. Taken together, the regional nature of this factor,
3 along with boundary layer effects help to explain this observed diurnal profile.

4 **Isoprene-epoxydiol organic aerosol (IEPOX-OA)**

5 Factors associated with IEPOX-derived SOA have been identified in a number of ambient field studies in the
6 southeastern USA (Budisulistiorini et al., 2016, 2013; Xu et al., 2015b), rural Canada (Slowik et al., 2011), a tropical forest
7 in Borneo, Malaysia (Robinson et al., 2011b, 2011a), and a tropical rainforest in the Amazon (Chen et al., 2015, 2009; de Sá
8 et al., 2017). Overall, these PMF studies have identified OA factors with an enhanced signal at m/z 82 in their OA mass
9 spectra. The major fragment contributing to m/z 82 is the $C_5H_6O^+$ fragment (m/z = 82.042).

10 The prominence of the m/z 82 peak in studies conducted in high-isoprene, low- NO_x environments has prompted the
11 use of $f_{C_5H_6O}$ (the fraction of the $C_5H_6O^+$ fragment to total OA) or f_{82} (fraction of m/z 82 to total OA) as a quantitative tracer
12 for SOA formed from IEPOX uptake (Allan et al., 2014; Hu et al., 2015). The anthropogenically-influenced/urban
13 background $f_{C_5H_6O}$ value, based on field studies using AMS measurements summarized in Hu et al. (2015), is $f_{C_5H_6O, Urban-Bkgrd} =$
14 0.0017 ± 0.0001 , while areas influenced by monoterpene emissions have higher background values of $f_{C_5H_6O, Monot.-Bkgrd} =$
15 0.0031 ± 0.0006 . The average value for PMF factors for ambient IEPOX-OA summarized in Hu et al. (2015) is $f_{C_5H_6O, IEPOX-OA PMF} = 0.022 \pm 0.007$. The authors hypothesize that: (1) the wide range of values for ambient IEPOX-OA PMF
16 factors (0.012 to 0.040) is indicative of the variability in the compounds that comprise IEPOX-OA and (2) ambient OA
17 oxidation processes or mixing with aged air masses can increase the fractional contribution of CO_2^+ while decreasing the
18 signature of IEPOX-OA of $C_5H_6O^+$. In this study, the campaign-averaged $f_{C_5H_6O}$ value is 0.0032, making it higher than the
19 urban background and consistent with the background value in areas influenced by monoterpene emissions. The $f_{C_5H_6O}$ for
20 A-IEPOX-OA and B-IEPOX-OA factors are 0.00622 and 0.00636, respectively. In total, the near-background campaign-
21 averaged $f_{C_5H_6O}$ and lower $f_{C_5H_6O, IEPOX-OA}$ for the PMF factors indicate that the OA at this site is potentially influenced by a
22 more aged IEPOX-OA. The notion of a transported/aged IEPOX-OA is also supported by Figure 2 in the main text, where
23 northeasterly and northwesterly two-day backward trajectories likely contribute to the IEPOX-OA loadings observed at the
24 site.

25
26 A-IEPOX-OA and B-IEPOX-OA represent 32.8% and 34.0% of the total OA mass for the above- and below-
27 canopy OA, respectively. IEPOX-OA is the least oxidized factor (O:C = 0.65). Its O:C value makes it a relatively fresh
28 OOA. A-IEPOX-OA and B-IEPOX-OA are also distinguished by signals at m/z 53 (mostly $C_4H_5^+$) and m/z 75 (mostly
29 $C_3H_7O_2^+$). The mass spectral characteristics at m/z 53, 75, and 82 are consistent with laboratory observations, where high
30 resolution mass spectra were generated by atomizing solutions of molecular IEPOX-SOA tracers and synthesized IEPOX
31 standards and analyzing them using AMS (Lin et al., 2012). Furthermore, comparison of the IEPOX-OA mass spectra with
32 reference mass spectra from ambient field studies in Atlanta, GA ($R = 0.88-0.94$) indicate similar mass spectra
33 (Budisulistiorini et al., 2013; Hu et al., 2015), as shown in Table S 6 and Table S 12.

34 The diurnal profiles of A-IEPOX-OA and B-IEPOX-OA (as shown in Figure 3 in the main text) reach a daily
35 maximum in the afternoon when photochemical activity is strongest, which is in general agreement with the diurnal profiles
36 of IEPOX-related factors in the southeastern US (Budisulistiorini et al., 2016; Xu et al., 2015b) and forests in the Amazon
37 (Chen et al., 2015). The A-IEPOX-OA and B-IEPOX-OA time series correlate with time series of $f_{C_5H_6O}$ ($R = 0.58$ and $R =$
38 0.54 , respectively). In addition, A-IEPOX-OA correlates with time series of above-canopy acetaldehyde measurements ($R =$
39 0.44), as shown in Table S 5. Compounds derived from isoprene oxidation observed at mass 136.07 ($C_5H_{12}O_4$; 2-
40 methyltetrols) are observed in PM_{10} filter sampling and HPLC-ESI-ToF-MS analysis by Yale University (Ditto et al., 2018).
41 Presence of this compound in PM_{10} provides evidence that isoprene oxidation products constitute a portion of the aerosol at
42 this site.

Previous source apportionment studies in the southeastern US have found that SO₄ aerosol is strongly correlated with IEPOX-OA (Budisulistiorini et al., 2013; Hu et al., 2015; Xu et al., 2015a, 2015b). In the work of Xu et al. (2015a), ambient isoprene SOA from IEPOX uptake was strongly associated with SO₄, due to the high abundance of SO₄ in the southeastern US and the nucleophilic strength of SO₄. The authors hypothesized that the nucleophilic strength of SO₄ facilitates the ring-opening reaction of IEPOX to form IEPOX-derived SOA. A comparison of the SO₄ concentration at this site to other sites in North America (where isoprene-derived SOA factors have been resolved) indicates relatively lower SO₄ mass concentrations (Budisulistiorini et al., 2016; Xu et al., 2015b). The resolved IEPOX-OA factor at this site has very weak correlations with SO₄ regardless of time of day and wind direction, but data indicates that there are subsets of the data in which SO₄ concentration may correlate with IEPOX-OA. Recent work from de Sá et al. (2017) in central Amazonia showed that NO_y concentrations helped to explain 75% of the variability in IEPOX-OA factor loadings in an environment where SO₄ concentrations were relatively lower (< 0.5 µg m⁻³) and more variable than that of the southeastern US. The authors hypothesized that elevated NO concentrations in urban-influenced plumes suppress IEPOX formation to a larger extent than SO₄ is able to enhance IEPOX formation, which implies that higher NO_y mixing ratios generally correspond to lower IEPOX-OA concentrations. For the PROPHET site, both a NO_y and temporal dependence on the relationship between SO₄ and IEPOX-OA is observed, however further work should focus on developing the relationships between NO_y and SO₄ on IEPOX formation at this site.

91 Factor (91Fac)

The A-91Fac and B-91Fac reported in this study is distinguished by a peak at m/z 91. The major fragments that contribute to m/z 91 are C₇H₇⁺ (100% of mass at m/z 91) and C₃H₉NO₂⁺. The C₇H₇⁺ fragment is also known as the tropylium ion, and has been identified as a fragment resulting from EI ionization of benzyl compounds (Lee et al., 2016; McLafferty and Turecek, 1993). Laboratory studies have identified characteristic peaks at m/z 91 as indicative NO₃⁻-initiated β-pinene SOA (Boyd et al., 2015), dark ozonolysis of β-caryophyllene (C₁₅H₂₄) (Chen et al., 2015), peroxide formation from low-NO_x isoprene environments (Surratt et al., 2006), pinonaldehyde uptake on acid seed aerosols (Liggio and Li, 2006), chamber SOA from a mixture of BVOCs from European and North American tree species (Kiendler-Scharr et al., 2009), and gas-phase oxidation of ISOPOOH resulting in isoprene-derived SOA through a non-IEPOX pathway (Riva et al., 2016).

The explicit formation pathway of 91Fac in the existing literature has remained unclear. Robinson et al. (2011) attributed 91Fac to aged biomass burning emissions over a Malaysian rain forest, due to its resemblance to biomass burning mass spectra. 91Fac, or OA factors with prominent peaks at m/z 91, have also been attributed to biogenic-influenced SOA chemistry in ambient field studies, such as monoterpene-related SOA in a coniferous forest in Whistler, British Columbia (Lee et al., 2016), freshly produced BVOC-derived SOA in the Amazon tropical rainforest based on mass spectra from chamber experiments (Chen et al., 2015), isoprene ozonolysis and photo-oxidation resulting in isoprene-SOA through a non-IEPOX pathway (Budisulistiorini et al., 2016), biogenic SOA in the boreal forests in Finland (Finessi et al., 2012), and biogenic SOA in the southeastern US (Rattanavaraha et al., 2017).

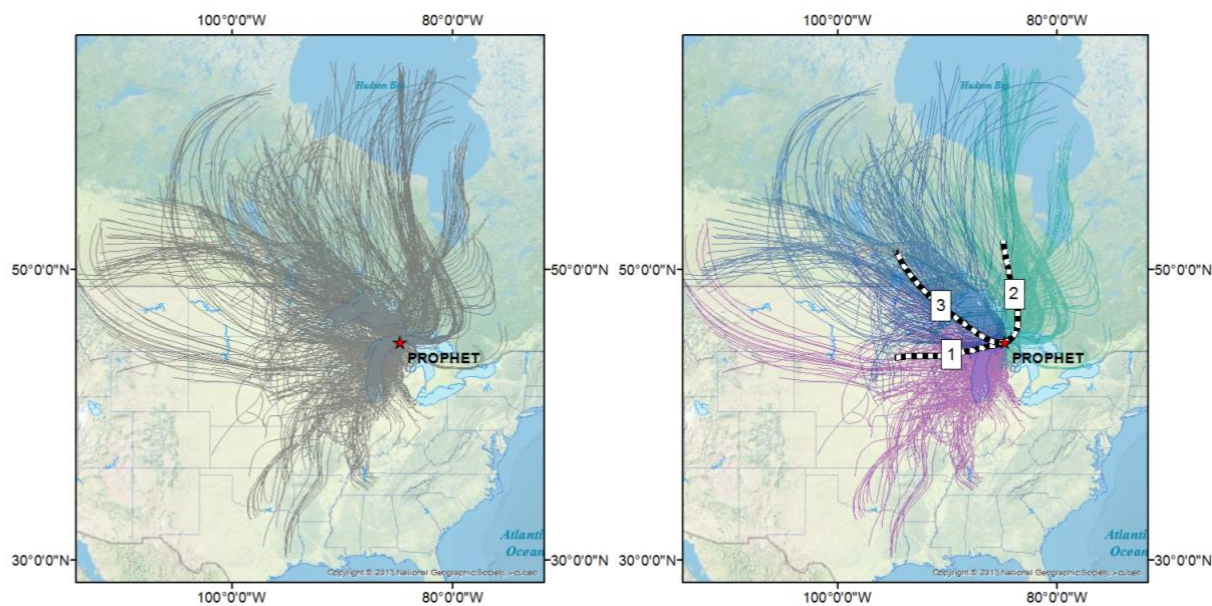
The fraction of the mass at m/z 91 (f₉₁) is 0.87% and 0.88% for A-91Fac and B-91Fac, respectively. The A-91Fac and B-91Fac factors both have an O:C of 0.69, which qualifies them as OOA. A-91Fac contributes 35.6% and 47.6% to the total OA mass for above and below the canopy, respectively. The time series of A-91Fac and B-91Fac correlate with VOC signals as detected by the PTR-QiTOF at the m/z values described in Table S 8 and Table S 13. The relative variability of the signal at these m/z values can be used as indicators for source apportionment analysis. A complete list of additional VOCs can be found in Table S 7. The C₉H₁₅O⁺ ion detected at mass 139.112 and the C₁₀H₁₇O₂⁺ at detected mass 169.122 are both identified as likely monoterpene oxidation products. Nopinone (a β-pinene oxidation product; (Atkinson and Arey, 2003; Kim et al., 2010; Lee et al., 2006a; Yuan et al., 2017)) and limona ketone (a limonene oxidation product, (Lee et al.,

1 2006b)) have both been observed at m/z 139.112, while pinonaldehyde (an α -pinene oxidation product; (Atkinson and Arey,
2 2003; Kim et al., 2010; Yuan et al., 2017)) and limonaldehyde (a limonene oxidation product; (Lee et al., 2006b)) have both
3 been observed at m/z 169.122. Temporal correlation of 91Fac with these detected VOC signals suggests similar formation
4 chemistry.

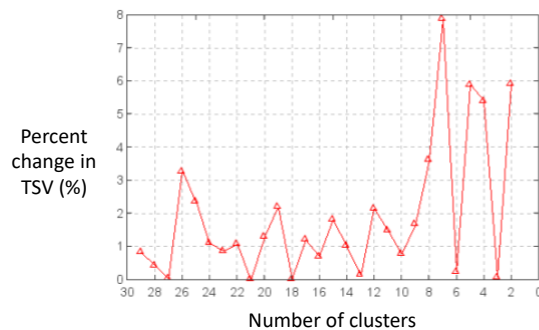
5 Monoterpene oxidation SOA tracers such as $C_{21}H_{28}O_6$, $C_9H_{14}O_4$, $C_9H_{14}O_4$ (pinic acid), and $C_{10}H_{16}O_3$ (pinonic acid)
6 were identified using PM_{10} filters and HPLC-ESI-QTOF analysis (Yale University). Previous laboratory studies have
7 identified low-volatility oxidation products of monoterpenes and O_3 (Draper et al., 2015; Ehn et al., 2012). The presence of
8 monoterpene SOA tracers, such as $C_{21}H_{28}O_6$ and $C_9H_{14}O_4$, and the detection of a number of other C_9 , C_{10} , C_{15} , and C_{21}
9 compounds in PM_{10} filters suggest that: (1) 91Fac is more closely tied to monoterpene-related SOA and (2) monoterpene
10 oxidation SOA is an observed fraction of the aerosol at the site. A full summary of the monoterpene-derived SOA tracer
11 species observed during the PROPHET-AMOS 2016 campaign can be found in the literature (Ditto et al., 2018).

12

1 **HYSPLIT backward trajectory analysis**



2
3 **Figure S 23: (left) Location of the PROPHET site (red star) with respect to 742 two-day backward trajectories (gray traces)**
4 **calculated using HYSPLIT, (right) Two-day backward trajectories are clustered into three trajectory clusters where Cluster#1**
5 **consists of 299 total backward-trajectories and represents southerly/southwesterly flow (magenta), Cluster #2 (192 backward-**
6 **trajectories) represents northeasterly flow (teal), and Cluster #3 (251 backward-trajectories) represents northwesterly flow (blue).**



7
8 **Figure S 24: Percent change in total spatial variation (TSV) versus number of backward-trajectory clusters ranging from 0 to 30**
9 **for backward-trajectories during the PROPHET AMOS 2016 campaign. Clustering of backward-trajectories was calculated**
10 **using the angle distance method (Sirois and Bottenheim, 1995). The angle distance method is appropriate for this study because**
11 **the main interest of using backward trajectories is to determine the direction from which air masses arrive at the site.**

12 Choosing the suitable number of trajectory clusters is based on two methods. The first method involves the plot of
13 percentage change in total spatial variation (TSV) versus number of clusters. Cluster numbers occurring *before* steep
14 increases in the percentage change in TSV correspond to “suitable” cluster numbers, where trajectories arriving at the site
15 originate from unique cluster directions. Figure S 24 indicates that for the PROPHET-AMOS campaign, clusters numbers 3,
16 6, 8, and 9 may be suitable choices. The second method involves a visual inspection of the mean trajectories plotted on a
17 map of the geographical source region (Sirois and Bottenheim, 1995). Mean cluster trajectories are calculated based on the

trajectories falling within their respective cluster. A determination using the second method is made based on the interpretability of the cluster mean trajectories, their relative spatial positioning, and overall trajectory shape. Overlapping mean cluster trajectories were observed for clusters 6, 8, and 9. Based on these two methods, three clusters are chosen for PROPHET-AMOS 2016.

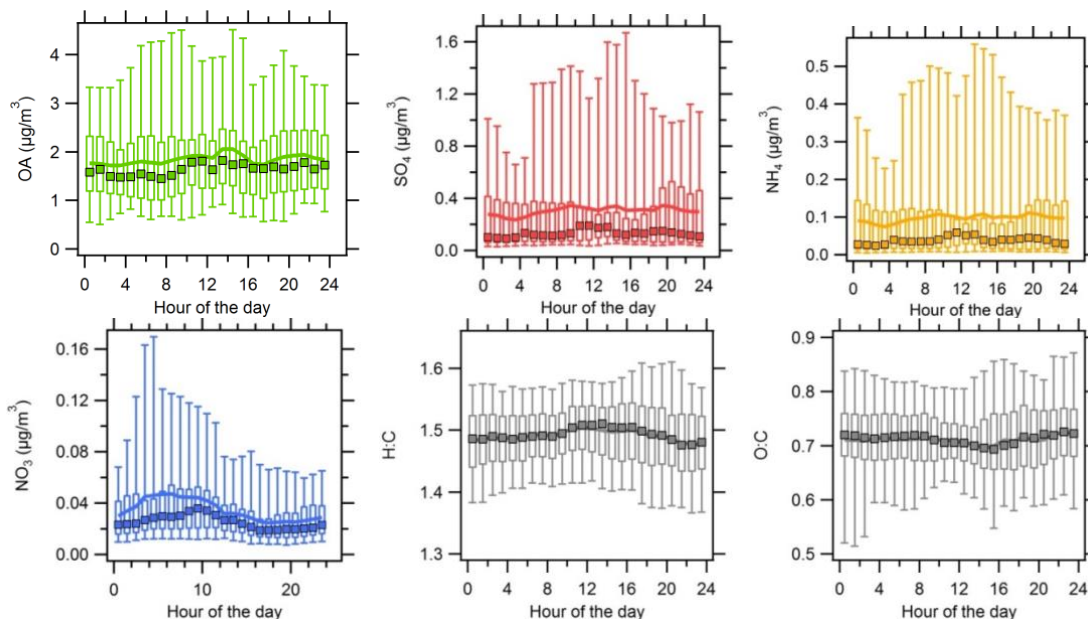


Figure S 25: Diurnal profiles of NR-PM₁ species and elemental ratios, as measured by HR-ToF-AMS, for (top panel from left to right) OA, SO₄, NH₄ and (bottom from left to right) NO₃, H:C, and O:C. The solid curves indicate average concentrations, squares represent median concentrations, upper and lower box borders represent 25th and 75th percentiles, respectively, and upper and lower whiskers represent 5th and 95th percentiles, respectively.

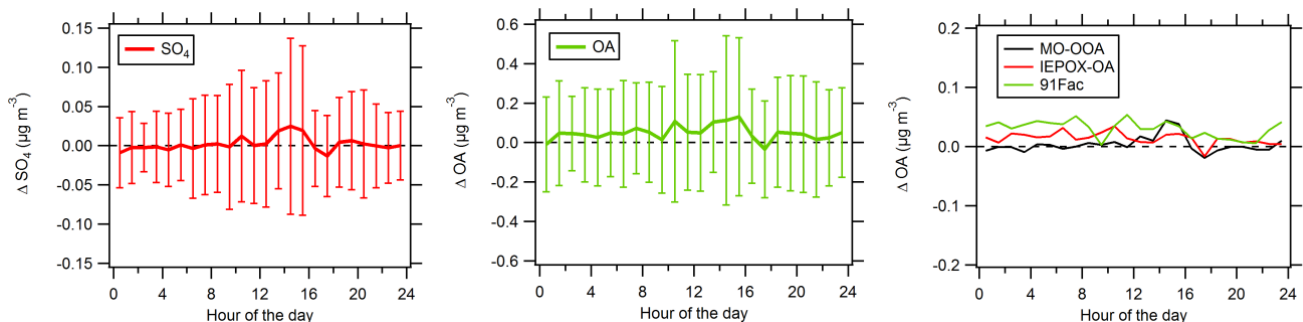


Figure S 26: Diel profiles of vertical differences from left to right, respectively: SO₄, OA, and OA factors. The solid lines indicate average concentrations and upper and lower whiskers represent one standard deviation from the mean (for the left and middle figures). Solid lines indicate the average concentrations for each OA factor (for the right figure).

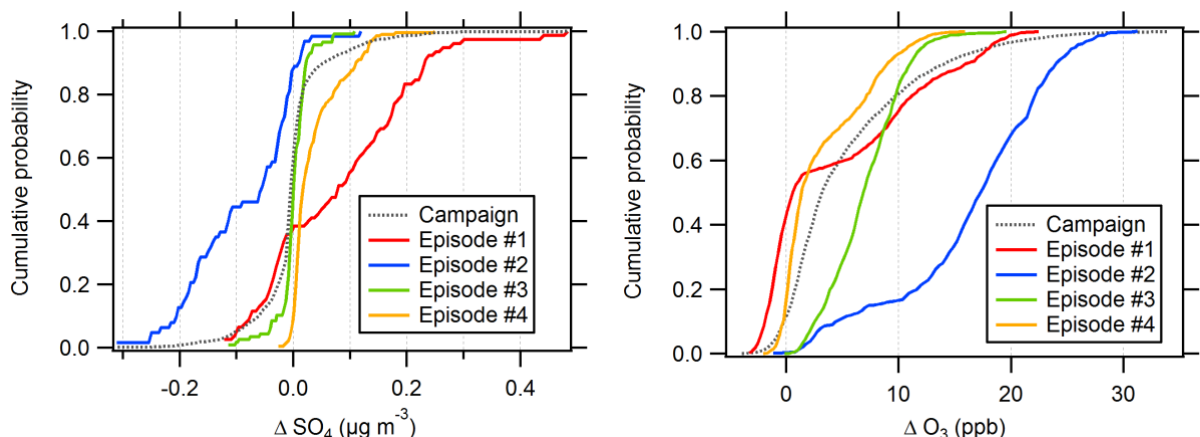


Figure S 27: Cumulative probability distributions for vertical differences episodes in (left) SO₄ and (right) O₃. Vertical differences in SO₄ were calculated using 30-minute averaged data from the above- and below-canopy AMS inlets on the PROPHET tower. Vertical differences in O₃ were calculated using 1-minute resolution data on the AmeriFlux tower. Episode data are shown with solid lines, and the full campaign data is shown with a dashed line.

1 **Particle deposition model parameters**

2 The particle dry deposition model used in this study is based on the resistance model outlined in Seinfeld and
3 Pandis (2006). This model assumes that the transport of particles from the atmosphere to a given surface (in the absence of
4 precipitation) is governed by three resistances in series: aerodynamic resistance, quasi-laminar layer resistance, and surface
5 or canopy resistance. The equations used for the resistance model for dry deposition can be found in Seinfeld and Pandis
6 (2006), and Table S 16 summarizes the parameters that were used in this study. Specific values from the deposition model in
7 Zhang et al. (2001) are used in this study that are representative of the land use category (LUC) and seasonal categories (SC)
8 at the PROPHET site.

9
10 **Table S 16: Parameters for dry deposition model**

Model input parameter:	Value:	Source:
Friction velocity (u^*)	0.1 m/s (low in-canopy mixing test case) 0.8 m/s (high in-canopy mixing test case)	This study
Standard acceleration due to gravity (g)	9.81 m/s ²	
Particle diameter (D_p)	1 μ m	This study
Temperature (T)	305 K	This study
Mean free path of air (λ)	6.98E-8 m	(Seinfeld and Pandis, 2006)
Atmospheric stability class	Stable	
Particle density (ρ)	1.4 g/cm ³	(Guo et al., 2015)
Height (z)	25 m (assumed vegetation canopy height)	This study
Roughness length (z_0)	1.05 m (LUC = deciduous broadleaf trees, SC = midsummer with lush vegetation)	(Zhang et al., 2001)
Monin-Obukhov length (L)	5 m	
von Karman constant (K)	0.41	
γ	0.56 (LUC = deciduous broadleaf trees))	(Zhang et al., 2001)
α	0.8 (LUC = 4, deciduous broadleaf trees)	(Zhang et al., 2001)
A	0.005 m (LUC = deciduous broadleaf trees, SC = midsummer with lush vegetation)	(Zhang et al., 2001)
Kinematic viscosity of air @ 298K	15.51E-6	
Boltzmann constant (k)	1.381E-23 J/K	(Seinfeld and Pandis, 2006)
$R1$	1.0 (parameter represents fraction of particles that stick to surface, assumed $R1 = 1$ for particles)	(Seinfeld and Pandis, 2006)
ϵ_0	Empirical constant	(Seinfeld and Pandis, 2006)
β	2	(Seinfeld and Pandis, 2006)

11
12

1 References

- 2 Allan, J.D., Morgan, W.T., Darbyshire, E., Flynn, M.J., Williams, P.I., Oram, D.E., Artaxo, P., Brito, J., Lee, J.D., Coe, H.,
3 2014. Airborne observations of IEPOX-derived isoprene SOA in the Amazon during SAMBBA. *Atmospheric*
4 *Chemistry and Physics* 14, 11393–11407. <https://doi.org/10.5194/acp-14-11393-2014>
- 5 Atkinson, R., Arey, J., 2003. Gas-phase tropospheric chemistry of biogenic volatile organic compounds: a review.
6 *Atmospheric Environment* 37, Supplement 2, 197–219. [https://doi.org/10.1016/S1352-2310\(03\)00391-1](https://doi.org/10.1016/S1352-2310(03)00391-1)
- 7 Atkinson, R., Baulch, D.L., Cox, R.A., Crowley, J.N., Hampson, R.F., Hynes, R.G., Jenkin, M.E., Rossi, M.J., Troe, J.,
8 2004. Evaluated kinetic and photochemical data for atmospheric chemistry: Volume I – gas phase reactions of O_x,
9 HO_x, NO_x and SO_x species. *Atmos. Chem. Phys* 4, 1461–1738. <https://doi.org/10.5194/acp-4-1461-2004>
- 10 Boyd, C.M., Sanchez, J., Xu, L., Eugene, A.J., Nah, T., Tuet, W.Y., Guzman, M.I., Ng, N.L., 2015. Secondary organic
11 aerosol formation from the β-pinene+NO₃ system: effect of humidity and peroxy radical fate. *Atmospheric*
12 *Chemistry and Physics* 15, 7497–7522. <https://doi.org/10.5194/acp-15-7497-2015>
- 13 Budisulistiorini, S.H., Baumann, K., Edgerton, E.S., Bairai, S.T., Mueller, S., Shaw, S.L., Knipping, E.M., Gold, A., Surratt,
14 J.D., 2016. Seasonal characterization of submicron aerosol chemical composition and organic aerosol sources in the
15 southeastern United States: Atlanta, Georgia, and Look Rock, Tennessee. *Atmospheric Chemistry and Physics* 16,
16 5171–5189. <https://doi.org/10.5194/acp-16-5171-2016>
- 17 Budisulistiorini, S.H., Canagaratna, M.R., Croteau, P.L., Marth, W.J., Baumann, K., Edgerton, E.S., Shaw, S.L., Knipping,
18 E.M., Worsnop, D.R., Jayne, J.T., Gold, A., Surratt, J.D., 2013. Real-Time Continuous Characterization of
19 Secondary Organic Aerosol Derived from Isoprene Epoxydiols in Downtown Atlanta, Georgia, Using the Aerodyne
20 Aerosol Chemical Speciation Monitor. *Environmental Science & Technology* 47, 5686–5694.
21 <https://doi.org/10.1021/es400023n>
- 22 Carroll, M.A., Bertman, S.B., Shepson, P.B., 2001. Overview of the Program for Research on Oxidants: PHotochemistry,
23 Emissions, and Transport (PROPHET) summer 1998 measurements intensive. *Journal of Geophysical Research*
24 106.
- 25 Chen, Q., Farmer, D.K., Rizzo, L.V., Pauliquevis, T., Kuwata, M., Karl, T.G., Guenther, A., Allan, J.D., Coe, H., Andreae,
26 M.O., Pöschl, U., Jimenez, J.L., Artaxo, P., Martin, S.T., 2015. Submicron particle mass concentrations and sources
27 in the Amazonian wet season (AMAZE-08). *Atmos. Chem. Phys.* 15, 3687–3701. [https://doi.org/10.5194/acp-15-](https://doi.org/10.5194/acp-15-3687-2015)
28 3687-2015
- 29 Chen, Q., Farmer, D.K., Schneider, J., Zorn, S.R., Heald, C.L., Karl, T.G., Guenther, A., Allan, J.D., Robinson, N., Coe, H.,
30 Kimmel, J.R., Pauliquevis, T., Borrmann, S., Pöschl, U., Andreae, M.O., Artaxo, P., Jimenez, J.L., Martin, S.T.,
31 2009. Mass spectral characterization of submicron biogenic organic particles in the Amazon Basin. *Geophys. Res.*
32 *Lett.* 36, L20806. <https://doi.org/10.1029/2009GL039880>
- 33 Crippa, M., Canonaco, F., Slowik, J.G., El Haddad, I., DeCarlo, P.F., Mohr, C., Heringa, M.F., Chirico, R., Marchand, N.,
34 Temime-Roussel, B., Abidi, E., Poulain, L., Wiedensohler, A., Baltensperger, U., Prévôt, A.S.H., 2013. Primary
35 and secondary organic aerosol origin by combined gas-particle phase source apportionment. *Atmospheric*
36 *Chemistry and Physics* 13, 8411–8426. <https://doi.org/10.5194/acp-13-8411-2013>
- 37 de Sá, S.S., Palm, B.B., Campuzano-Jost, P., Day, D.A., Newburn, M.K., Hu, W., Isaacman-VanWertz, G., Yee, L.D.,
38 Thalman, R., Brito, J., Carbone, S., Artaxo, P., Goldstein, A.H., Manzi, A.O., Souza, R.A.F., Mei, F., Shilling, J.E.,
39 Springston, S.R., Wang, J., Surratt, J.D., Alexander, M.L., Jimenez, J.L., Martin, S.T., 2017. Influence of urban
40 pollution on the production of organic particulate matter from isoprene epoxydiols in central Amazonia. *Atmos.*
41 *Chem. Phys.* 17, 6611–6629. <https://doi.org/10.5194/acp-17-6611-2017>
- 42 Ditto, J.C., Barnes, E.B., Khare, P., Takeuchi, M., Joo, T., Bui, A.A.T., Lee-Taylor, J., Eris, G., Chen, Y., Aumont, B.,
43 Jimenez, J.L., Ng, N.L., Griffin, R.J., Gentner, D.R., 2018. An omnipresent diversity and variability in the chemical
44 composition of atmospheric functionalized organic aerosol. *Communications Chemistry* 1, 75.
45 <https://doi.org/10.1038/s42004-018-0074-3>
- 46 Draper, D.C., Farmer, D.K., Desyaterik, Y., Fry, J.L., 2015. A qualitative comparison of secondary organic aerosol yields
47 and composition from ozonolysis of monoterpenes at varying concentrations of NO₂. *Atmospheric Chemistry and*
48 *Physics* 15, 12267–12281. <https://doi.org/10.5194/acp-15-12267-2015>

1 Ehn, M., Kleist, E., Junninen, H., Petäjä, T., Lönn, G., Schobesberger, S., Dal Maso, M., Trimborn, A., Kulmala, M.,
2 Worsnop, D.R., Wahner, A., Wildt, J., Mentel, Th.F., 2012. Gas phase formation of extremely oxidized pinene
3 reaction products in chamber and ambient air. *Atmos. Chem. Phys.* 12, 5113–5127. [https://doi.org/10.5194/acp-12-](https://doi.org/10.5194/acp-12-5113-2012)
4 5113-2012

5 Finessi, E., Decesari, S., Paglione, M., Giulianelli, L., Carbone, C., Gilardoni, S., Fuzzi, S., Saarikoski, S., Raatikainen, T.,
6 Hillamo, R., Allan, J., Mentel, Th.F., Tiitta, P., Laaksonen, A., Petäjä, T., Kulmala, M., Worsnop, D.R., Facchini,
7 M.C., 2012. Determination of the biogenic secondary organic aerosol fraction in the boreal forest by NMR
8 spectroscopy. *Atmos. Chem. Phys.* 12, 941–959. <https://doi.org/10.5194/acp-12-941-2012>

9 Geddes, J.A., Murphy, J.G., 2014. Observations of reactive nitrogen oxide fluxes by eddy covariance above two midlatitude
10 North American mixed hardwood forests. *Atmospheric Chemistry and Physics* 14, 2939–2957.
11 <https://doi.org/10.5194/acp-14-2939-2014>

12 Guo, H., Xu, L., Bougiatioti, A., Cerully, K.M., Capps, S.L., Hite, J.R., Carlton, A.G., Lee, S.-H., Bergin, M.H., Ng, N.L.,
13 Nenes, A., Weber, R.J., 2015. Fine-particle water and pH in the southeastern United States. *Atmospheric Chemistry*
14 *and Physics* 15, 5211–5228. <https://doi.org/10.5194/acp-15-5211-2015>

15 Hao, L.Q., Kortelainen, A., Romakkaniemi, S., Portin, H., Jaatinen, A., Leskinen, A., Komppula, M., Miettinen, P., Sueper,
16 D., Pajunoja, A., Smith, J.N., Lehtinen, K.E.J., Worsnop, D.R., Laaksonen, A., Virtanen, A., 2014. Atmospheric
17 submicron aerosol composition and particulate organic nitrate formation in a boreal forestland–urban mixed region.
18 *Atmospheric Chemistry and Physics* 14, 13483–13495. <https://doi.org/10.5194/acp-14-13483-2014>

19 Hu, W.W., Campuzano-Jost, P., Palm, B.B., Day, D.A., Ortega, A.M., Hayes, P.L., Krechmer, J.E., Chen, Q., Kuwata, M.,
20 Liu, Y.J., de Sá, S.S., McKinney, K., Martin, S.T., Hu, M., Budisulistiorini, S.H., Riva, M., Surratt, J.D., St. Clair,
21 J.M., Isaacman-Van Wertz, G., Yee, L.D., Goldstein, A.H., Carbone, S., Brito, J., Artaxo, P., de Gouw, J.A., Koss,
22 A., Wisthaler, A., Mikoviny, T., Karl, T., Kaser, L., Jud, W., Hansel, A., Docherty, K.S., Alexander, M.L.,
23 Robinson, N.H., Coe, H., Allan, J.D., Canagaratna, M.R., Paulot, F., Jimenez, J.L., 2015. Characterization of a real-
24 time tracer for isoprene epoxydiols-derived secondary organic aerosol (IEPOX-SOA) from aerosol mass
25 spectrometer measurements. *Atmospheric Chemistry and Physics* 15, 11807–11833. [https://doi.org/10.5194/acp-15-](https://doi.org/10.5194/acp-15-11807-2015)
26 11807-2015

27 Jimenez, J.L., Canagaratna, M.R., Donahue, N.M., Prevot, A.S.H., Zhang, Q., Kroll, J.H., DeCarlo, P.F., Allan, J.D., Coe,
28 H., Ng, N.L., Aiken, A.C., Docherty, K.S., Ulbrich, I.M., Grieshop, A.P., Robinson, A.L., Duplissy, J., Smith, J.D.,
29 Wilson, K.R., Lanz, V.A., Hueglin, C., Sun, Y.L., Tian, J., Laaksonen, A., Raatikainen, T., Rautiainen, J.,
30 Vaattovaara, P., Ehn, M., Kulmala, M., Tomlinson, J.M., Collins, D.R., Cubison, M.J., E., Dunlea, J., Huffman,
31 J.A., Onasch, T.B., Alfarra, M.R., Williams, P.I., Bower, K., Kondo, Y., Schneider, J., Drewnick, F., Borrmann, S.,
32 Weimer, S., Demerjian, K., Salcedo, D., Cottrell, L., Griffin, R., Takami, A., Miyoshi, T., Hatakeyama, S.,
33 Shimono, A., Sun, J.Y., Zhang, Y.M., Dzepina, K., Kimmel, J.R., Sueper, D., Jayne, J.T., Herndon, S.C., Trimborn,
34 A.M., Williams, L.R., Wood, E.C., Middlebrook, A.M., Kolb, C.E., Baltensperger, U., Worsnop, D.R., 2009.
35 Evolution of Organic Aerosols in the Atmosphere. *Science* 326, 1525–1529.
36 <https://doi.org/10.1126/science.1180353>

37 Kiendler-Scharr, A., Zhang, Q., Hohaus, T., Kleist, E., Mensah, A., Mentel, T.F., Spindler, C., Uerlings, R., Tillmann, R.,
38 Wildt, J., 2009. Aerosol Mass Spectrometric Features of Biogenic SOA: Observations from a Plant Chamber and in
39 Rural Atmospheric Environments. *Environ. Sci. Technol.* 43, 8166–8172. <https://doi.org/10.1021/es901420b>

40 Kim, S., Karl, T., Guenther, A., Tyndall, G., Orlando, J., Harley, P., Rasmussen, R., Apel, E., 2010. Emissions and ambient
41 distributions of Biogenic Volatile Organic Compounds (BVOC) in a ponderosa pine ecosystem: interpretation of
42 PTR-MS mass spectra. *Atmospheric Chemistry and Physics* 10, 1759–1771. [https://doi.org/10.5194/acp-10-1759-](https://doi.org/10.5194/acp-10-1759-2010)
43 2010

44 Lanz, V.A., Alfarra, M.R., Baltensperger, U., Buchmann, B., Hueglin, C., Prévôt, A.S.H., 2007. Source apportionment of
45 submicron organic aerosols at an urban site by factor analytical modelling of aerosol mass spectra. *Atmos. Chem.*
46 *Phys.* 7, 1503–1522. <https://doi.org/10.5194/acp-7-1503-2007>

47 Lee, A., Goldstein, A.H., Keywood, M.D., Gao, S., Varutbangkul, V., Bahreini, R., Ng, N.L., Flagan, R.C., Seinfeld, J.H.,
48 2006a. Gas-phase products and secondary aerosol yields from the ozonolysis of ten different terpenes. *J. Geophys.*
49 *Res.* 111, D07302. <https://doi.org/10.1029/2005JD006437>

- 1 Lee, A., Goldstein, A.H., Kroll, J.H., Ng, N.L., Varutbangkul, V., Flagan, R.C., Seinfeld, J.H., 2006b. Gas-phase products
2 and secondary aerosol yields from the photooxidation of 16 different terpenes. *Journal of Geophysical Research*
3 111. <https://doi.org/10.1029/2006JD007050>
- 4 Lee, A.K.Y., Abbatt, J.P.D., Leaitch, W.R., Li, S.-M., Sjostedt, S.J., Wentzell, J.J.B., Liggio, J., Macdonald, A.M., 2016.
5 Substantial secondary organic aerosol formation in a coniferous forest: observations of both day- and nighttime
6 chemistry. *Atmospheric Chemistry and Physics* 16, 6721–6733. <https://doi.org/10.5194/acp-16-6721-2016>
- 7 Liggio, J., Li, S.-M., 2006. Organosulfate formation during the uptake of pinonaldehyde on acidic sulfate aerosols. *Geophys.*
8 *Res. Lett.* 33, L13808. <https://doi.org/10.1029/2006GL026079>
- 9 Lin, Y.-H., Zhang, Z., Docherty, K.S., Zhang, H., Budisulistiorini, S.H., Rubitschun, C.L., Shaw, S.L., Knipping, E.M.,
10 Edgerton, E.S., Kleindienst, T.E., Gold, A., Surratt, J.D., 2012. Isoprene Epoxydiols as Precursors to Secondary
11 Organic Aerosol Formation: Acid-Catalyzed Reactive Uptake Studies with Authentic Compounds. *Environmental*
12 *Science & Technology* 46, 250–258. <https://doi.org/10.1021/es202554c>
- 13 McLafferty, F.W., Turecek, F., 1993. Interpretation of mass spectra. University Science Books, Mill Valley, California.
- 14 Millet, D.B., Alwe, H.D., Chen, X., Deventer, M.J., Griffis, T.J., Holzinger, R., Bertman, S.B., Rickly, P.S., Stevens, P.S.,
15 Léonardis, T., Locoge, N., Dusanter, S., Tyndall, G.S., Alvarez, S.L., Erickson, M.H., Flynn, J.H., 2018.
16 Bidirectional Ecosystem–Atmosphere Fluxes of Volatile Organic Compounds Across the Mass Spectrum: How
17 Many Matter? *ACS Earth and Space Chemistry* 2, 764–777. <https://doi.org/10.1021/acsearthspacechem.8b00061>
- 18 Mohr, C., DeCarlo, P.F., Heringa, M.F., Chirico, R., Slowik, J.G., Richter, R., Reche, C., Alastuey, A., Querol, X., Seco, R.,
19 Peñuelas, J., Jiménez, J.L., Crippa, M., Zimmermann, R., Baltensperger, U., Prévôt, A.S.H., 2012. Identification
20 and quantification of organic aerosol from cooking and other sources in Barcelona using aerosol mass spectrometer
21 data. *Atmospheric Chemistry and Physics* 12, 1649–1665. <https://doi.org/10.5194/acp-12-1649-2012>
- 22 Ng, N.L., Canagaratna, M.R., Jimenez, J.L., Zhang, Q., Ulbrich, I.M., Worsnop, D.R., 2011. Real-Time Methods for
23 Estimating Organic Component Mass Concentrations from Aerosol Mass Spectrometer Data. *Environmental*
24 *Science & Technology* 45, 910–916. <https://doi.org/10.1021/es102951k>
- 25 Ng, N.L., Canagaratna, M.R., Zhang, Q., Jimenez, J.L., Tian, J., Ulbrich, I.M., Kroll, J.H., Docherty, K.S., Chhabra, P.S.,
26 Bahreini, R., Murphy, S.M., Seinfeld, J.H., Hildebrandt, L., Donahue, N.M., DeCarlo, P.F., Lanz, V.A., Prévôt,
27 A.S.H., Dinar, E., Rudich, Y., Worsnop, D.R., 2010. Organic aerosol components observed in Northern
28 Hemispheric datasets from Aerosol Mass Spectrometry. *Atmospheric Chemistry and Physics* 10, 4625–4641.
29 <https://doi.org/10.5194/acp-10-4625-2010>
- 30 Raatikainen, T., Vaattovaara, P., Tiitta, P., Miettinen, P., Rautiainen, J., Ehn, M., Kulmala, M., Laaksonen, A., Worsnop,
31 D.R., 2010. Physicochemical properties and origin of organic groups detected in boreal forest using an aerosol mass
32 spectrometer. *Atmospheric Chemistry and Physics* 10, 2063–2077. <https://doi.org/10.5194/acp-10-2063-2010>
- 33 Rattanavaraha, W., Canagaratna, M.R., Budisulistiorini, S.H., Croteau, P.L., Baumann, K., Canonaco, F., Prevot, A.S.H.,
34 Edgerton, E.S., Zhang, Z., Jayne, J.T., Worsnop, D.R., Gold, A., Shaw, S.L., Surratt, J.D., 2017. Source
35 apportionment of submicron organic aerosol collected from Atlanta, Georgia, during 2014–2015 using the aerosol
36 chemical speciation monitor (ACSM). *Atmospheric Environment* 167, 389–402.
37 <https://doi.org/10.1016/j.atmosenv.2017.07.055>
- 38 Riva, M., Budisulistiorini, S.H., Chen, Y., Zhang, Z., D’Ambro, E.L., Zhang, X., Gold, A., Turpin, B.J., Thornton, J.A.,
39 Canagaratna, M.R., Surratt, J.D., 2016. Chemical Characterization of Secondary Organic Aerosol from Oxidation of
40 Isoprene Hydroxyhydroperoxides. *Environmental Science & Technology* 50, 9889–9899.
41 <https://doi.org/10.1021/acs.est.6b02511>
- 42 Robinson, N.H., Hamilton, J.F., Allan, J.D., Langford, B., Oram, D.E., Chen, Q., Docherty, K., Farmer, D.K., Jimenez, J.L.,
43 Ward, M.W., Hewitt, C.N., Barley, M.H., Jenkin, M.E., Rickard, A.R., Martin, S.T., McFiggans, G., Coe, H.,
44 2011a. Evidence for a significant proportion of Secondary Organic Aerosol from isoprene above a maritime tropical
45 forest. *Atmos. Chem. Phys.* 11, 1039–1050. <https://doi.org/10.5194/acp-11-1039-2011>
- 46 Robinson, N.H., Newton, H.M., Allan, J.D., Irwin, M., Hamilton, J.F., Flynn, M., Bower, K.N., Williams, P.I., Mills, G.,
47 Reeves, C.E., McFiggans, G., Coe, H., 2011b. Source attribution of Bornean air masses by back trajectory analysis
48 during the OP3 project. *Atmos. Chem. Phys.* 11, 9605–9630. <https://doi.org/10.5194/acp-11-9605-2011>
- 49 Rupakheti, M., Leaitch, W.R., Lohmann, U., Hayden, K., Brickell, P., Lu, G., Li, S.-M., Toom-Sauntry, D., Bottenheim,
50 J.W., Brook, J.R., Vet, R., Jayne, J.T., Worsnop, D.R., 2005. An Intensive Study of the Size and Composition of

- Submicron Atmospheric Aerosols at a Rural Site in Ontario, Canada. *Aerosol Science and Technology* 39, 722–736. <https://doi.org/10.1080/02786820500182420>
- Seinfeld, J.H., Pandis, S.N., 2006. *Atmospheric Chemistry and Physics: From Air Pollution to Climate Change*, 2nd Edition. Wiley.
- Sirois, A., Bottenheim, J.W., 1995. Use of backward trajectories to interpret the 5-year record of PAN and O₃ ambient air concentrations at Kejimikujik National Park, Nova Scotia. *Journal of Geophysical Research* 100, 2867. <https://doi.org/10.1029/94JD02951>
- Slowik, J.G., Brook, J., Chang, R.Y.-W., Evans, G.J., Hayden, K., Jeong, C.-H., Li, S.-M., Liggio, J., Liu, P.S.K., McGuire, M., Mihele, C., Sjostedt, S., Vlasenko, A., Abbatt, J.P.D., 2011. Photochemical processing of organic aerosol at nearby continental sites: contrast between urban plumes and regional aerosol. *Atmospheric Chemistry and Physics* 11, 2991–3006. <https://doi.org/10.5194/acp-11-2991-2011>
- Slowik, J.G., Stroud, C., Bottenheim, J.W., Brickell, P.C., Chang, R.-W., Liggio, J., Makar, P.A., Martin, R.V., Moran, M.D., Shantz, N.C., others, 2010. Characterization of a large biogenic secondary organic aerosol event from eastern Canadian forests. *Atmospheric Chemistry and Physics* 10, 2825–2845. <https://doi.org/10.5194/acp-10-2825-2010>
- Surratt, J.D., Murphy, S.M., Kroll, J.H., Ng, N.L., Hildebrandt, L., Sorooshian, A., Szmigielski, R., Vermeylen, R., Maenhaut, W., Claeys, M., Flagan, R.C., Seinfeld, J.H., 2006. Chemical Composition of Secondary Organic Aerosol Formed from the Photooxidation of Isoprene. *The Journal of Physical Chemistry A* 110, 9665–9690. <https://doi.org/10.1021/jp061734m>
- Ulbrich, I.M., Canagaratna, M.R., Zhang, Q., Worsnop, D.R., Jimenez, J.L., 2009. Interpretation of organic components from Positive Matrix Factorization of aerosol mass spectrometric data. *Atmospheric Chemistry and Physics* 9, 2891–2918.
- Vlasenko, A., Slowik, J.G., Bottenheim, J.W., Brickell, P.C., Chang, R.Y.-W., Macdonald, A.M., Shantz, N.C., Sjostedt, S.J., Wiebe, H.A., Leaitch, W.R., Abbatt, J.P.D., 2009. Measurements of VOCs by proton transfer reaction mass spectrometry at a rural Ontario site: Sources and correlation to aerosol composition. *J. Geophys. Res.* 114, D21305. <https://doi.org/10.1029/2009JD012025>
- Xu, L., Guo, H., Boyd, C.M., Klein, M., Bougiatioti, A., Cerully, K.M., Hite, J.R., Isaacman-VanWertz, G., Kreisberg, N.M., Knote, C., Olson, K., Koss, A., Goldstein, A.H., Hering, S.V., de Gouw, J., Baumann, K., Lee, S.-H., Nenes, A., Weber, R.J., Ng, N.L., 2015a. Effects of anthropogenic emissions on aerosol formation from isoprene and monoterpenes in the southeastern United States. *Proceedings of the National Academy of Sciences* 112, 37–42. <https://doi.org/10.1073/pnas.1417609112>
- Xu, L., Suresh, S., Guo, H., Weber, R.J., Ng, N.L., 2015b. Aerosol characterization over the southeastern United States using high-resolution aerosol mass spectrometry: spatial and seasonal variation of aerosol composition and sources with a focus on organic nitrates. *Atmospheric Chemistry and Physics* 15, 7307–7336. <https://doi.org/10.5194/acp-15-7307-2015>
- Yuan, B., Koss, A.R., Warneke, C., Coggon, M., Sekimoto, K., de Gouw, J.A., 2017. Proton-Transfer-Reaction Mass Spectrometry: Applications in Atmospheric Sciences. *Chem. Rev.* <https://doi.org/10.1021/acs.chemrev.7b00325>
- Zhang, L., Gong, S., Padro, J., Barrie, L., 2001. A size-segregated particle dry deposition scheme for an atmospheric aerosol module. *Atmospheric Environment* 35, 549–560. [https://doi.org/10.1016/S1352-2310\(00\)00326-5](https://doi.org/10.1016/S1352-2310(00)00326-5)